Geophysical signatures of mineral deposit types in Finland
Edited by Meri-Liisa Airo
Geological Survey of Finland, Special Paper 58, 117–144, 2015

HYPERSPECTRAL CLOSE-RANGE LWIR IMAGING SPECTROMETRY – 3 CASE STUDIES

by

Viljo Kuosmanen[1], Hilkka Arkimaa[1], Markku Tiainen[1] and Rainer Bärs[2]

Kuosmanen, V. , Arkimaa, H., Tiainen, M. & Bärs, R. 2015. Hyperspectral close-range LWIR Imaging spectrometry – 3 case studies. *Geological Survey of Finland, Special Paper 58*, 117–144, 14 figures and 6 tables.

Long wavelength infra-red (LWIR) imaging spectrometry data acquired with the SisuROCK instrument were tested for their ability to estimate mineral abundances in rock samples. Three diverse targets were selected to test the method. The targets were the Kemi chrome mine, the Pyhäsalmi Cu-Zn-S mine and the Kedonojankulma Cu-Au ore prospect. In Kemi, the scope was to determine whether the ore types and a few host rocks were distinguishable by LWIR. In Pyhäsalmi and Kedonojankulma, the main focus of the study was on the identification of the alteration minerals amongst other minerals. A set of exploration drilling powders from Pyhäsalmi was also included in the study. Their mineral abundances and three main chemical commodities, Cu, Zn and S, were additionally estimated.

Partial least squares regression (PLSR) and linear unmixing regression (UMXR) successfully predicted the quantities of those minerals that were 'sufficiently present'. In the Kemi case, these were: actinolite, albite, chlorite, chromite, dolomite, epidote, magnesite, quartz, serpentine, talc and tremolite. In the Pyhäsalmi and Kedonojankulma cases, they were: albite, allanite, biotite, chalcopyrite, cordierite, ilmenite, K-feldspar, laumontite, muscovite, phlogopite, plagioclase and quartz. These could be quantified with a fairly small risk, i.e. mean absolute error (MAE) ≤ 16%, Pearson correlation coefficient (CC) ≥ 0.4 and p-value ≤ 0.05. Those minerals that classify the ore types and wall rocks in the Kemi case and the main and alteration minerals in the Pyhäsalmi and Kedonojankulma cases belong to the list of the predictable minerals. In the Kemi case, the predictable minerals are: actinolite, albite, chlorite, chromite, dolomite, epidote, magnesite, quartz, serpentine, talc and tremolite. In the Pyhäsalmi and Kedonojankulma cases, they are: albite, biotite, chalcopyrite, cordierite, K-feldspar, muscovite, phlogopite, plagioclase and quartz.

PLSR and UMXR produced mutually coincident results. The accuracy for the sample composition prediction was seemingly better than that for a single mineral prediction on average. The reason for this is that the minor minerals that are present in mineral prediction are 'nearly absent' in sample composition prediction. The main minerals, including the alteration minerals, and their unknown new mixtures can be quantified using this technique with moderate accuracy, which benefits mineral exploration and mining actions.

Keywords (GeoRef Thesaurus, AGI): minerals, quantitative analysis, remote sensing, hyperspectral analysis, image analysis, spectroscopy, Kemi, Pyhäsalmi, Kedonojankulma, Finland

1 Geological Survey of Finland, P.O. Box 96, FI-02151 Espoo, Finland
2 Specim Oy, Elektroniikkatie 13, P.O. Box 110, FI-90590 Oulu, Finland

E-mail: viljo.kuosmanen@gtk.fi, hilkka.arhimaa@gtk.fi, markku.tiainen@gtk.fi

INTRODUCTION

Remote sensing and analysis involves measuring and studying samples of light and nearby electromagnetic radiation reflected or emitted from a target at varying wavelengths, preferably from 0.3 microns to 20 microns (300 to 20 000 nanometers). The variety of absorption processes and their wavelength dependence allows us to obtain information on the abundances of minerals. Due to the varying molecular structure of different minerals, their reflectance/emittance characteristics are expressed by the respective wavelengths of electromagnetic radiation. Traditionally, two parts of that wavelength area are used for mineral mapping: visible to short wavelength infrared (VSWIR, 0.3–2.5 microns) and long wavelength infrared (LWIR, 3–14 micron) areas. The VSWIR area is sensitive, for example, to clay minerals, micas, chlorites, carbonates, talc, sulphates and iron oxides, and the LWIR area is sensitive, for example, to quartz, feldspars, garnet, olivine, pyroxenes and oxides. Therefore, the VSWIR and LWIR areas highly complement each other in remote sensing.

If the remote sensor is able to scan from tens to hundreds of contiguous channels of the electromagnetic spectrum, it is defined as a hyperspectral remote sensor or an imaging spectrometer (IS). The SisuROCK (Specim Oy, Oulu, Finland) sensor is able to conduct close-range hyperspectral 'remote' sensing.

The rapid mineral mapping method using reflected and emitted hyperspectral SWIR and LWIR wavelengths of electromagnetic radiation has been introduced to mineral mining and exploration markets. At present, this hyperspectral method does not compete with the classical mineral identification methods (e.g. SEM, X-ray diffraction or MLA) as an accurate tool on a per-sample basis. However, the hyperspectral method will soon develop towards the full detection of mineral species over large sets of samples or geological surfaces. The hyperspectral method is by far the most rapid one, capable of measuring millions of spectra as pixels per minute. Furthermore, abundant minerals with developing accuracy can be quantified from the spectra. Therefore, it is important to be prepared for its utilization.

Hyperspectral close-range drill core imaging and wall rock imaging and analysis were first conducted using the PIMA spectrometer (Kruse 1996). The mining industry uses hyperspectral data for operational exploration, separation and concentration purposes. Both lateral and vertical hyperspectral close-range imaging spectrometry of rocks have been reported (Gallie et al. 2002, Bolin and Moon 2003, Ragona et al. 2006, Brown et al. 2008). These papers report that the hyperspectral imaging of rocks and rock surfaces is a very promising technique to estimate mineralogical continua, and to bridge the gap between geological point measurement and image data. It was demonstrated quite early that the number of minerals that can be detected and quantified is markedly increased by the use of thermal infrared wavelengths (Abrams et al. 1991, Hook and Kahle 1996). Thermal remote sensing of rocks was greatly developed by Salisbury et al. (1989) and Salisbury and Daria (1992).

Currently, the SisuROCK is the only commercial instrument offering a thermal (LWIR) imaging option. The commercial HyLogger (Mason & Huntington 2012) offers only a point-measurement thermal spectrometer, capturing profile-type spectral data. The Aerospace Corporation started the development of a research-type instrument named SEBASS (Spatially Enhanced Broadband Array Spectrograph System) in 1993 (Taranik et al. 2008), which has also been used in geological remote sensing and close range mineral scanning tests (Kirkland et al. 2002).

The methods used for processing imaging spectrometry data from drillcores are mostly the same as are known to the remote sensing community: spectrum matching techniques and subpixel methods (van der Meer 2006). We are especially interested in the added value of LWIR for quantitative mineral estimation, because there have been no previous publishes cases in Finland and a few in the entire world. The main interest here is, of course, to reveal the precision of the estimates of minerals.

The purpose of this study was to test and develop the interpretation of the LWIR close-range remote sensing technique for the rapid mapping of rocks and minerals in diverse mining environments. Therefore, sample sets were selected from four diverse targets: the layered intrusion-hosted Kemi Cr ore, the volcanogenic massive sulphide-type Pyhäsalmi Cu-Zn-S ore related altered country rocks, the granitoid-hosted Kedonojankulma Cu-Au ore prospect and Pyhäsalmi ore exploration

drilling powders. The samples of the current study were related to mining technology aspects rather than forming a complete set covering the whole geological regime. This study consisted of the following tasks:

- Classification of the mineral/rock samples separately using their MLA and LWIR data;
- Testing chances for quantitative mineral detection using LWIR data;
- Assessment of the accuracy of mineral quantity prediction.

This paper introduces the one way to use LWIR imaging spectrometry for mining operations and geological studies. The SisuROCK hyperspectral core logging workstation, which contains an LWIR imaging spectrometer, is described. The LWIR reflectance/emissivity spectra of the targets are described in reference to the international spectral libraries and the current measurements. A dedicated LWIR spectral library (in SisuROCK wavelength domain) has been built for the Kemi, Pyhäsalmi and Kedonojankulma cases. The geology of the ore deposits is briefly described, as well as the criteria for the selection of the samples. The main part of this report concerns the classification of rock types and the quantitative prediction minerals from the precision point of view. The prediction methods are partial linear unmixing regression (UMXR) and partial nonlinear least squares regression (PLSR). The results are validated in relation to the reference measurements, prediction of minerals and the prediction methods used.

METHODS

Imaging spectrometry using SisuROCK applied to Kemi, Pyhäsalmi and Kedonojankulma samples

SisuROCK, developed by Specim Oy (Oulu, Finland), is a fully automated hyperspectral imaging workstation for easy and high-speed scanning of drill cores. Depending on the application, SisuROCK contains a combination of the following spectral cameras: VNIR (0.4–1.0 μm), SWIR (0.97–2.5 μm), combined VNIR+SWIR (0.38–2.5 μm), LWIR (8–12 μm) and a high-resolution RGB camera. LWIR (long wave infrared) or thermal spectra usually cover the electromagnetic spectrum between 3.0–15.0 μm. For the current study, the SisuROCK OWL instrument measured the thermal spectrum between 7.065–12.35 μm. SisuROCK collects spectral and spatial information on drillcores as the core tray is automatically moved through the system. All cameras are push-broom cameras, meaning that they image a single, full image line across the target, and the target is moved under the camera to create a 2D spatial image with full spectral information for each spatial pixel. The hyperspectral imaging data of a whole core tray is acquired in less than 2 minutes. The spatial pixel size is 0.96 x 0.96 mm^2. The detailed specifications are provided on the manufacturer's website (www.Specim.fi).

The SisuROCK LWIR imaging for the current study was carried out on 16 June 2014 by the company Specim Oy in Oulu, Finland (http://specim.fi/index.php/products/geology/sisurock/). The samples were laid in two black-painted, otherwise normal drill core trays (37.0 x 103.7 cm in size), with each tray consisting of six sites for the cores/samples. The rock samples were dry and clean in the sense that they were kept in dry indoor temperatures and conditions for weeks and smoothly brushed before scanning. An automatic conveyor belt carried the trays under the field-of-view of the spectrometer. The sample set in the drill core trays contained the following (the numbers refer to Fig. 1):

- Pure mineral 'markers' (numbers 1–18, 90), powder/block (mainly ground pure mineral crystals) ;
- Ore concentrates from Kemi and Pyhäsalmi mines (20–23), powder
- Drilling powder from the Pyhäsalmi Cu-Zn-S mine (24–59, 106–107), powder
- Samples of Kemi Cr ore and host rocks (60–70, 80–89, 98–105), block and drill core
- Pyhäsalmi samples related to alteration studies (71–79, 91), drill cores
- Pyhäsalmi samples related to alteration studies (108–122), drill 'chips'
- Kedonojankulma samples related to alteration studies (92–97, 123–153), drill cores.

The marker minerals were (from 1 to 18): plagioclase (50% An), serpentine (antigorite), albite and

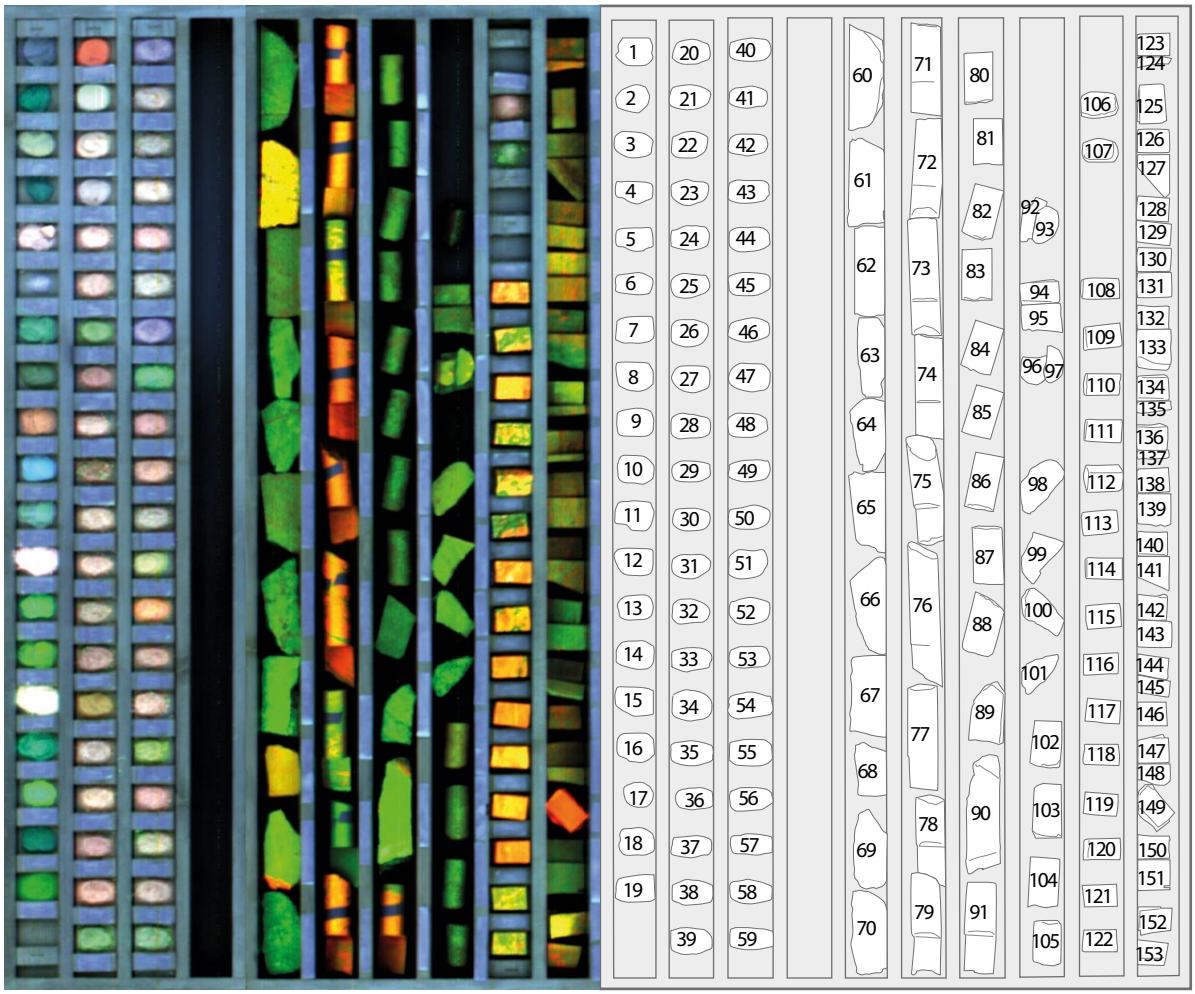

Fig. 1. A composite picture of all samples: The SisuROCK LWIR image (left) and their ID numbers (right). The mineral/chemical contents of most of the samples can be found in GTK's archives with these numbers. The colours of the LWIR image represent wavelength bands 8386 nm, 10162 nm and 11985 nm (r, g and b, respectively).

serpentine from Kemi mine, graphite, magnesite, biotite, hornblende, cordierite, apatite, phlogopite, dolomite, tremolite, chlorite (group), calcite, talc, garnet (almandine) and muscovite. Number 19 is an industrial smelted impure feldspar and not therefore used here.

The scanning produced a 117-band LWIR-image matrix for both trays. These two images were mosaicked into one combined SisuROCK LWIR image for the current studies (Fig. 1, left). This entire study was based on this image. The drawing on the right shows the sample locations and numbers that refer to the stored mineral/chemical reference data.

Preprocessing from raw data to reflectance and corrections for blinking pixels

The reflectance R is defined as the fraction of the total infrared light irradiance, incident on the surface plane of the material, that is reflected back. For the total incident light on the surface of a material:

Reflectance + Absorbance + Transmittance = 100%

The SisuROCK hyperspectral raw data (= image, dark, white [DN]) was directly transformed to reflectance, R, using the following formula:

R = (image – dark)/(white – dark) , 0≤R ≤1. We denote for clarity: R x 10000. = X0, and later in this report, X0 is also called reflectance.

The conversion of the recorded signal to reflectance removes the camera and illumination functions from the acquired data, leaving only the target material response.

The captured white reference is used as an absolute reference signal to scale the input data. The white reference target consists of a panel sheet with known, high (~100%) reflectance over the full wavelength range and reflects all wavelengths (nearly) evenly to the sensor. The dark reference level is obtained by closing the camera shutter, thereby obtaining a signal level corresponding to absolute darkness, or for thermal measurements, alternatively imaging a room-temperature dark cavity, giving the background thermal signal. This dark level was subtracted from the scanned image and from the response of the white reference. Thereafter, these magnitudes were mutually ratioed. Therefore, R is a dimensionless parameter. It describes the target's ability to reflect/emit electromagnetic radiation as a function of wavelength, in 117 wavelengths bands between 7065–12 350 nm. Reflectance was computed separately for each pixel in order to remove the variation due to individual detector pixels. Both the white and dark references were measured during each scan to remove time-dependent variation in the signal. After some noisy channels were omitted, those images that contained the planned sample set from the test areas were mosaicked into one 632 x 977 x 86 (columns x lines x bands) image. The mosaic was split into one-test-area images when necessary.

According to López-Alonso and Alda (2002), the number of bad or blinking pixels is a quality figure that defines a given detector array. However, the exact definition of a bad pixel is not standardized; it differs depending on the author of the paper. Usually, it is possible to define three types of bad pixels depending on how the output signal of the pixel depends on the number of photons (light) collected: (1) 'always on' or 'always off' pixels are those that always produce the same signal, (2) noisy pixels are those having noise greater than a fixed threshold, and (3) blinking or drifting pixels are those having temporal behaviour clearly different from those considered as good pixels. However, this classification is not universal and strongly depends on the context.

The 'blinking' or 'bad' pixel phenomenon exists in most camera detectors to a varying degree, and also in the thermal images recorded by SisuROCK. This means that the output signal intensity of a number of pixels in the 2D detector matrix does not depend on the number of photons collected. In spectral images, these can be seen as stripes in a spatial image, or peak noise in pixel spectra. These erroneous signals were filtered by calculating a moving median over three consecutive channels along the spectral dimension.

Spectral libraries

Several LWIR spectral libraries are available for the public use. A large number of emissivity spectra of minerals, rocks, vegetation and man-made objects have been collected in the ASTER library (Balridge et al. 2009). The ENVI + IDL image processing environment (Exelis/Harris Corporation, Melbourne Florida, USA) contains several spectral collections for minerals. The VSWIR area is commonly well represented, but the thermal domain is not evenly covered. The spectra may contain gaps and the data from different sources for a single mineral species are often based on different spectral sampling. The ENVI spectral library was studied in detail and the suitable material was included and scaled into the same spectral domain with the SisuROCK data. However, the analysis of the quantities is mainly based on the SisuROCK spectra.

A dedicated spectral library for the current Kemi and Pyhäsalmi-Kedonojankulma SisuROCK studies was built using the marker minerals (samples 1–18) in the combined sample image and other samples with the highest possible single mineral content (samples 80, 90 and 149). The dedicated LWIR spectral library is archived in the permanent computer storage at the Geological Survey of Finland.

Ancillary measurements

Samples as targets for various measurements

The sampling strategy was based on selecting a representative set of rocks from the diverse mining domains. All 153 samples (see Fig. 1) from the test sites were measured with the SisuROCK OWL scanner. The mineralogy of most of the samples was also assayed by other methods, which are briefly introduced in the later sections. It is important to note that the part of a sample exposed to

various assay methods was not exactly the same. The SisuROCK data are imported for computing through hand-drawn windows on the image of the samples. These windows are called regions of interest (ROIs). The ROIs were drawn in such a way that maximal reflectance information from any sample is transmitted to computing, but not the background and the shadowed parts of the rocks. The size of the ROIs varied from 500 mm^2 to 1800 mm^2. The non-coincidence of these two types of windows is naturally a source of 'small' errors.

Mineral liberation analysis, MLA

The mineral content of the chosen model targets in the combined sample set of the current study was determined by the mineral liberation analysis (MLA) method. It is a scanning electron microscope FEI Quanta 600, equipped with energy dispersive X-ray (EDX) spectrometers (Sylvester 2012). MLA is an automated mineral analysis system that can identify minerals in the polished sections of drill core, particulate or lump materials, and quantify a wide range of mineral characteristics, such as mineral species abundance, grain size and liberation. From the total of 153 samples, 108 were subjected to mineralogical assays by MLA, which scanned the sample from a window, the size of which is constantly 707 mm^2. The MLA analyses were used as ancillary response data in building the regression models for the mineral prediction. The current samples are mainly homogeneous, fine or medium grained, and the MLA measurement is consequently considered to represent the whole ROI. Therefore, the non-coincidence error between the ROI domain and the MLA domain is small.

X-ray diffraction and XRF chemical analyser

X-ray diffraction (XRD) methods were used to verify the 18 marker minerals species and in a few cases for small spots of rock samples to identify unknown minerals (http://en.gtk.fi/research/infrastructure/researchlaboratory/XRD.html).

During this study, the DELTA Handheld XRF Analyzer (OLYMPUS, Tokyo, Japan) was used for chemical element analysis of the rock drilling powder samples. The handheld XRF is a fast and cost-effective way to identify and quantify the content of models used in interpretation (http://www.olympus-ims.com/en/xrf-xrd/delta-handheld /). The measurements were repeated 4–10 times in order to minimize the error in the analysis. Most of the drilling powder samples (nos. 25–59, 106, 107) were analysed by Pyhäsalmi Mine Oy, but the concentrates (nos. 20-23) were analysed by XRF. The XRD and XRF measurement were in practice not used in the statistical prediction; they were only used to ensure the mineral species/element content in specific cases.

A quantitative interpretation method for LWIR reflectance data on rocks

Notations and preprocesses

In this report, the LWIR SisuROCK reflectance spectra of the samples are denoted as $\boldsymbol{X_0}$ ($0. \le \boldsymbol{X_0} \le 10000.$ [DN]) and the MLA mineral compositions of the same samples are denoted as $\boldsymbol{Y_0}$ ($0. \le \mathbf{Y_0} \le 100.$[area %]).

The frequency of a mineral for the variable $\boldsymbol{Y_0}$ and for the estimated results is here expressed in 'area units' [au]. The sum area for a mineral simply means the integrated mineral percentage from the MLA assays through the sample set under examination. The full content of one sample is 100% (± a small assay error) and it is equal to 100 au. We assume that the total MLA focus area on the chip of a sample is a constant 706.86 mm^2. Therefore 1 au = 7.0686 mm^2 = 7.6136 pixels in SisuROCK terms.

Because the characteristic LWIR features for minerals are mostly indicated by fluctuations in the reflectance/emittance curve, those fluctuations are optionally enhanced here to maximize the discernibility of the minerals. For this purpose, a three-term high-pass (Pratt 2001) component $\boldsymbol{r_1}$ was first computed for $\boldsymbol{X_0}$, multiplied by a constant $0 \le f \le 100$ and added to the original curve before the next steps. If the components of $\boldsymbol{X_0}$ are $a_1, a_2, \ldots, a_k$, then the high-pass component $\boldsymbol{r}$ is defined by the moving residual, where the general term of $\boldsymbol{r}$ is defined by $r_n = a_n - (a_{n-1} + a_n + a_{n+1})/3$, $(n \le k)$, except that the first and last terms are truncated. The constant f varies from 0% to 1% from the maximum reflectance 10000 , i.e. $0 \le f \le 100$. The constant f for each case was computed by minimizing the estimation errors. The enhanced spectrum is thereafter denoted as $\boldsymbol{X_1} = \boldsymbol{X_0} + f\,\boldsymbol{r}$.

Unsupervised hierarchical clustering was used here to foresee the true mineralogical clusters of the samples ($\boldsymbol{Y}_0$) and compare them with the spectral ($\boldsymbol{X}_1$) clusters of the samples. This connectivity based clustering software/procedure was here assembled from the available interactive data language (IDL) tools. The distance between elements of each cluster was used to compute the dendrogram, a 'cluster tree', which reveals the mutual hierarchy of the mineralogy and the mean spectra separately. The input for the clustering is a vector containing the pairwise distance matrix in compact form. Given a set of m items of $\boldsymbol{Y}_0$ or $\boldsymbol{X}_1$, with the distance between items i and j denoted by D(i, j), pairdistance should be an m(m-1)/2 element vector, ordered as: [D(0, 1), D(0, 2), ..., D(0, m-1), D(1, 2), ..., D(m-2, m)]. Single linkage of nearest neighbour was used here for computing the link distances between clusters for the dendrogram.

Unmixing and partial least squares regression

Mineral quantities were here estimated from the optionally filtered mean spectra of the ROIs ($\boldsymbol{X}_{1R}$) or the pixel spectra ($\boldsymbol{X}_{1P}$) and the mineral data $\boldsymbol{Y}_0$ using two methods. These were the classical unmixing (UMX) regression (UMXR) (Nielsen 1999) and partial least squares (PLS) regression (PLSR; Wold 1975, Geladi and Kowalski 1986). The role of UMX was to cross-validate the results from the PLS method. Mineralogy and analytical chemistry normally use sharp absorption peaks for the identification of species of minerals or elements and their quantities. Both PLSR and UMXR can, instead of the sharp peaks, utilize the soft variation in absorption to identify minerals or elements and their quantities.

The final estimation of quantities is based on the (optionally filtered) LWIR ROI spectra or pixel spectra as the predictor variables $\boldsymbol{X} = \boldsymbol{X}_{1R}$ or $\boldsymbol{X} = \boldsymbol{X}_{1P}$. Mineral compositions are the response variables $\boldsymbol{Y} = \boldsymbol{Y}_0$. In the usual multiple linear regression context (UMXR), the least-squares solution (Mevik and Wehrens 2007, Wold et al. 2001) for

$$\boldsymbol{Y} = \boldsymbol{XB} + \boldsymbol{\varepsilon} \quad (2)$$

is given by the regression model $\boldsymbol{B}$

$$\boldsymbol{B} = (\boldsymbol{X}^T\boldsymbol{X})^{-1}\boldsymbol{X}^T\boldsymbol{Y} \quad (3)$$

Because the regression is mostly carried out with least squares, there will be a residual term $\varepsilon \neq 0$. The problem is often that $\boldsymbol{X}^T\boldsymbol{X}$ is singular, either because the number of variables in $\boldsymbol{X}$ exceeds the number of samples or because of collinearities (Mevik and Wehrens 2007) between the variables.

PLSR is a widely used method in chemometrics, economics, and in medical and even social sciences. This approach is suitable for interpreting spectra that are highly correlated, or nearly singular matrices may occur in the procedure for calculating the regression between the predictor $\boldsymbol{X}$ and response variables $\boldsymbol{Y}$ (Wold et al. 2001).

The PLS procedure divides both $\boldsymbol{X}$ and $\boldsymbol{Y}$ into matrix components called scores and loadings by singular value decomposition (Wold 1975, Mevik and Wehrens 2007):

$$\boldsymbol{X} = \boldsymbol{WT} + \varepsilon_x \quad (4)$$

$$\boldsymbol{Y} = \boldsymbol{PQ} + \varepsilon_y \quad (5)$$

The scores $\boldsymbol{W}$ and $\boldsymbol{P}$ and loadings $\boldsymbol{T}$ and $\boldsymbol{Q}$ are calculated iteratively to maximally describe the covariance between $\boldsymbol{X}$ and $\boldsymbol{Y}$ (Wold 1975, Mevik and Wehrens 2007). We denote

$\boldsymbol{R} = \boldsymbol{W}(\boldsymbol{P}^T\boldsymbol{W})^{-1}$ then the regression term $\boldsymbol{B}$ is:

$$\boldsymbol{B} = \boldsymbol{R}\,(\boldsymbol{T}^T\boldsymbol{T})^{-1}\boldsymbol{T}^T\boldsymbol{Y} = \boldsymbol{RQ}^T \quad (6)$$

The advantage of PLSR is that the method does not necessarily need to know the spectra of the end members, i.e. the 'outermost' features in the spectral data space, as model inputs. The disadvantage of both methods is that they may produce negative 'concentrations'. The residual error term ε is uniquely expressed by the mean absolute error (MAE) and the root mean square error (RMSE). The calibration-validation error as a function of the number of samples decreases very quickly in PLSR (Krämer and Sugiyama 2011). Success in the PLSR and UMX predictions is inversely proportional to the residual error terms ε_y (RMSE and MAE) and the p-value, but proportional to the Pearson correlation coefficient (CC). All these parameters were computed for each prediction. The p-value states the risk (from 0 to 1) taken by the parameters MAE, RMSE, and CC.

The PLSR method has successfully been used for the interpretation of mineral quantities of rocks and elemental quantities in soils (Hecker et al. 2012, Middleton et al. 2011). For the current use, the UMXR and PLSR modelling methods

were coded in IDL programming language by the first author.

In practical work, we first estimated the content of all minerals within each sample represented by the ROI. Secondly, we needed to know the precision for each single mineral estimate. The mineral content is the most important information for a mining geologist and mining processes, but the parameter 'content' can only be utilized in the framework of the precision computed. Both the content and the precision parameters are computed in the same run by the PLSR (and UMXR) regression software: The mineral estimates are obtained from the rows and ROI estimates are obtained from the columns of the resulting prediction matrix. The precision estimates are obtained as residuals from the rows or columns respectively. However, because the precision of the estimates was the main target of this study, the results are represented here mainly in the light of precision and reliability parameters.

SAMPLE MATERIALS

The crucial question of this report is whether the LWIR method together with PLSR interpretation works in totally dissimilar environments. This question dictated the selection of samples from diverse environments, the Kemi and Pyhäsalmi mines and the Kedonojankulma ore prospect. The sample types were also diverse: hand specimens, dill cores and drilling powders.

Brief geological description of the Kemi chrome deposit and the selection of characteristic samples from the mine for the current study

The Kemi chrome mine is located near the town of Kemi in NW Finland, in the western part of the Tornio-Näränkävaara belt (Alapieti 2005). The substantial chromitite deposit is hosted by a layered intrusion, a chromitite layer in the lower ultramafic part of the intrusion (Alapieti and Huhtelin 2005, Iljina and Hanski 2005). U-Pb zircon data yield an Archaean age of 2.44 Ga for the Kemi intrusion (Kouvo 1977).

The 29 samples from the Kemi mine were selected by the mining experts Timo Huhtelin (pers. comm. 2014) and Ossi Leinonen (pers. comm. 2001). This sample set was not aimed to represent the whole geological regime, but instead to represent a variety of ores, soft, medium and hard ore types, and examples of wall rocks. The set of samples consisted of chromite-talc-carbonate-type soft ore, chromite-chlorite soft ore, chromite-serpentine hard ore, tremolite-chlorite-carbonate wall rocks and mafic/felsic wall rocks.

Geological description and the background for the sample selection from Pyhäsalmi and Kedonojankulma

The Pyhäsalmi Cu-Zn-S mine is located in the Pyhäjärvi commune, in the Svecofennian Proterozoic schist belt. The rocks in the area are granitoidic, dioritic and gabbroic magmatic plutonic rocks, volcanogenic felsic and mafic rocks and sedimentogenic migmatized gneisses (Korsman et al. 1997). The ore deposit is related to strong hydrothermal activity induced by bimodal volcanism, which started from the felsic type and changed into the mafic type as it continued (Mäki 1986, Kousa et al. 1997). The alteration mineralogy of the volcanites shows that the K- and Mg-enrichment in felsic volcanites correlates with quantities of sericite, cordierite, phlogopite and chlorite. Correspondingly, in mafic volcanites, the amount of cordierite, followed by chlorite, amphibole and phlogopite, is the best indicator for the alteration intensity (Puustjärvi 1999). The Pyhäsalmi samples for the current study were selected from the alteration zones around the ore deposit, bearing in mind the need to test the possibilities for mapping the alteration minerals by LWIR modelling. Altogether, 15 drill core samples from Pyhäsalmi were examined (received from J. Kousa pers comm. 2013 and Timo Mäki pers comm. 2013).

The Kedonojankulma Cu-Au ore prospect is located in the Forssa region in the municipality of Jokioinen, southern Finland. The discovered Cu-Au(-Ag-Mo) occurrence is hosted by a porphyric granitoid intrusion in the Palaeoproterozoic volcanic-intrusive Häme belt, part of the Southern Svecofennian Arc Complex in southern Finland. The fine-grained mineralization is controlled by a veined fractured and sheared, strongly altered zone in the quartz-plagioclase porphyry. The Kedonojankulma occurrence has several features that are typical of porphyry style Cu deposits. The most prominent are the metal contents and zoning, with Cu-Au-Ag-As-Mo in the core, Mo and Cu in quartz veins outside of the core and Zn-Cu-Ag in the outer zone of the intrusion. Various alteration assemblages in the mineralized zone have been identified, with silicification, chloritization, sericitization and epidotization being common (Tiainen et al. 2012, Tiainen et al. 2013).

The assumed genetic ore type of the Kedonojankulma prospect differs from the Pyhäsalmi case, but, the alteration mineralogy is partly the same and these Pyhäsalmi and Kedonojankulma alteration-related samples were therefore decided to examine jointly in the current study.

RESULTS AND DISCUSSION

Mineralogical clusters of the Kemi samples inferred from MLA

The frequent minerals encountered in the MLA studies of the Kemi samples were actinolite, albite, chlorite, chromite, biotite, calcite, dolomite, diopside, epidote, hornblende, K-feldspar, magnesite, muscovite, phlogopite, plagioclase, quartz, serpentine, talc and tremolite. Their area exceeded 1% at least in some of the samples. Chromite was mainly composed of the chromite-Mg type. Small quantities of chromite-Fe and chromite-Ti were also found, and included in the entity of 'chromite'. In

Kemi mineral prediction

Mineral index	Mineral	PLS MAE%	PLS RMSE%	PLS CC	Predictv ROIs	S-area [au]	p-value
1	**Actinolite**	**3.05**	**4.49**	**0.65**	**28**	**47.87**	**0.0001**
2	**Albite**	**4.87**	**8.84**	**0.85**	**28**	**142.39**	**0.0000**
3	**Chlorite**	**10.46**	**12.98**	**0.37**	**28**	**420.76**	**0.0499**
4	**Chromite**	**15.02**	**20.46**	**0.76**	**28**	**1019.60**	**0.0000**
5	Biotite	2.28	5.01	0.12	28	24.94	0.5450
6	Calcite	2.04	4.73	0.10	28	15.69	0.5902
7	**Dolomite**	**1.28**	**1.57**	**0.84**	**28**	**66.48**	**0.0000**
8	Diopside	2.02	3.42	-0.03	28	15.78	0.8735
9	**Epidote**	**2.05**	**3.07**	**0.52**	**28**	**24.61**	**0.0040**
10	Hornblende	1.34	2.23	0.04	28	7.70	0.8451
11	K_feldspar	1.10	2.73	-0.05	28	12.90	0.8133
12	**Magnesite**	**2.90**	**3.46**	**0.90**	**28**	**118.28**	**0.0000**
13	Muscovite	0.88	2.19	-0.03	28	10.41	0.8720
14	Phlogopite	5.54	7.91	0.06	28	50.01	0.7526
15	Plagioclase	1.35	2.00	-0.02	28	6.74	0.9199
16	**Quartz**	**2.36**	**5.18**	**0.85**	**28**	**71.49**	**0.0000**
17	**Serpentine**	**4.13**	**5.04**	**0.96**	**28**	**363.70**	**0.0000**
18	**Talc**	**3.23**	**4.47**	**0.94**	**28**	**298.17**	**0.0000**
19	**Tremolite**	**8.48**	**11.51**	**0.64**	**28**	**170.18**	**0.0002**
	Total area [au]					**2887.69**	

Table 1. The statistical descriptors for the mineral prediction by partial least squares regression (PLSR) in the Kemi case. Mineral indices are in the left column (for Figure 6). The mean absolute errors (MAEs) and root mean squared errors (RMSEs) are only acceptable for the bolded minerals. The low correlation coefficient (CC) and high p-value value exclude those minerals for which the prediction is not reliable.

addition, very small quantities of other minerals were found, such as ankerite, apatite, chalcopyrite, chamosite, iddingsite, ilmenite, magnetite, magnetite-Cr, millerite, monazite, pyrite, pyrrhotite, rutile, sphalerite, titanite, zircon and pentlandine.

In Table 1, the column 'S-area' presents the frequency [au] of the named, most important minerals in this set of the Kemi samples determined by the MLA assays. Albite, chlorite, chromite, dolomite, magnesite, phlogopite, serpentine, talc and tremolite appear in the set of samples several times.

Figure 2 presents a dendrogram, i.e. an illustration of the results from the Kemi MLA mineral

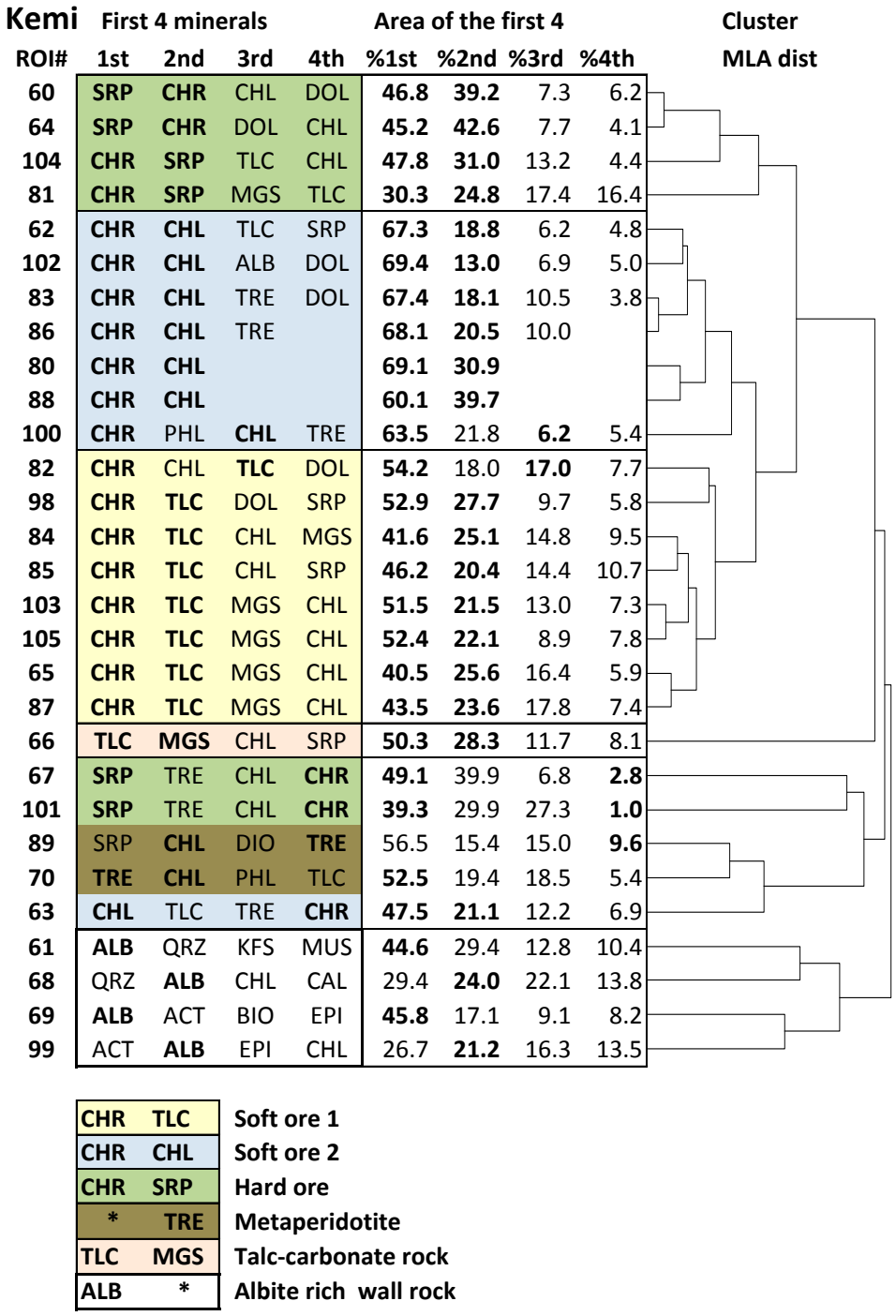

Kemi	First 4 minerals				Area of the first 4				Cluster
ROI#	1st	2nd	3rd	4th	%1st	%2nd	%3rd	%4th	MLA dist
60	**SRP**	**CHR**	CHL	DOL	**46.8**	**39.2**	7.3	6.2	
64	**SRP**	**CHR**	DOL	CHL	**45.2**	**42.6**	7.7	4.1	
104	**CHR**	**SRP**	TLC	CHL	**47.8**	**31.0**	13.2	4.4	
81	**CHR**	**SRP**	MGS	TLC	**30.3**	**24.8**	17.4	16.4	
62	**CHR**	**CHL**	TLC	SRP	**67.3**	**18.8**	6.2	4.8	
102	**CHR**	**CHL**	ALB	DOL	**69.4**	**13.0**	6.9	5.0	
83	**CHR**	**CHL**	TRE	DOL	**67.4**	**18.1**	10.5	3.8	
86	**CHR**	**CHL**	TRE		**68.1**	**20.5**	10.0		
80	**CHR**	**CHL**			**69.1**	**30.9**			
88	**CHR**	**CHL**			**60.1**	**39.7**			
100	**CHR**	PHL	**CHL**	TRE	**63.5**	21.8	**6.2**	5.4	
82	**CHR**	CHL	**TLC**	DOL	**54.2**	18.0	**17.0**	7.7	
98	**CHR**	**TLC**	DOL	SRP	**52.9**	**27.7**	9.7	5.8	
84	**CHR**	**TLC**	CHL	MGS	**41.6**	**25.1**	14.8	9.5	
85	**CHR**	**TLC**	CHL	SRP	**46.2**	**20.4**	14.4	10.7	
103	**CHR**	**TLC**	MGS	CHL	**51.5**	**21.5**	13.0	7.3	
105	**CHR**	**TLC**	MGS	CHL	**52.4**	**22.1**	8.9	7.8	
65	**CHR**	**TLC**	MGS	CHL	**40.5**	**25.6**	16.4	5.9	
87	**CHR**	**TLC**	MGS	CHL	**43.5**	**23.6**	17.8	7.4	
66	**TLC**	**MGS**	CHL	SRP	**50.3**	**28.3**	11.7	8.1	
67	**SRP**	TRE	CHL	**CHR**	**49.1**	39.9	6.8	**2.8**	
101	**SRP**	TRE	CHL	**CHR**	**39.3**	29.9	27.3	**1.0**	
89	SRP	**CHL**	DIO	**TRE**	56.5	15.4	15.0	**9.6**	
70	**TRE**	**CHL**	PHL	TLC	**52.5**	19.4	18.5	5.4	
63	**CHL**	TLC	TRE	**CHR**	**47.5**	**21.1**	12.2	6.9	
61	**ALB**	QRZ	KFS	MUS	**44.6**	29.4	12.8	10.4	
68	QRZ	**ALB**	CHL	CAL	29.4	**24.0**	22.1	13.8	
69	**ALB**	ACT	BIO	EPI	**45.8**	17.1	9.1	8.2	
99	ACT	**ALB**	EPI	CHL	26.7	**21.2**	16.3	13.5	

CHR	**TLC**	**Soft ore 1**
CHR	**CHL**	**Soft ore 2**
CHR	**SRP**	**Hard ore**
*	**TRE**	**Metaperidotite**
TLC	**MGS**	**Talc-carbonate rock**
ALB	*	**Albite rich wall rock**

Fig. 2. A dendrogram illustration for a classification of the MLA measurements of the samples from the Kemi mine. Different types of wall rocks and ores are separated, with a few exceptions. The marker mineral combination is bolded for each type. Abbreviations are: ALB = albite, ACT = actionlite, BIO = biotite, CAL = calcite, CHL = chlorite, CHR = chromite, DIO = diopside, DOL = dolomite, EPI = epidote, KFS = K-feldspar, MGS = magnesite, PHL = phlogopite, QRZ = quartz, SRP = serpentine, TLC = talc, TRE = tremolite.

data clustering. Different types of wall rocks and ore are separated in this sample set. Soft ore is divided into chromite-talc-carbonate type and chromite-chlorite type. Hard ore is seen as chromite-serpentine composite. The wall rock types are albite-dominant rock, talc-carbonate rock and metaperidotite in this sample set.

Contribution of the SisuROCK LWIR assays to the estimation of mineral quantities from the Kemi samples

Apparent mineralogical clusters inferred from the Kemi LWIR mean spectra

The filtered (constant f = 100.) LWIR mean spectra (Fig. 3) from the Kemi sample set were hierarchically clustered. The dendrogram in Figure 4 illustrates the clusters and the internal hierarchy of the LWIR spectra and possibly apparent rock types (cf. Fig. 2). The main classes are separated by the spectra, but a few exceptions occur. The internal hierarchies are about similar.

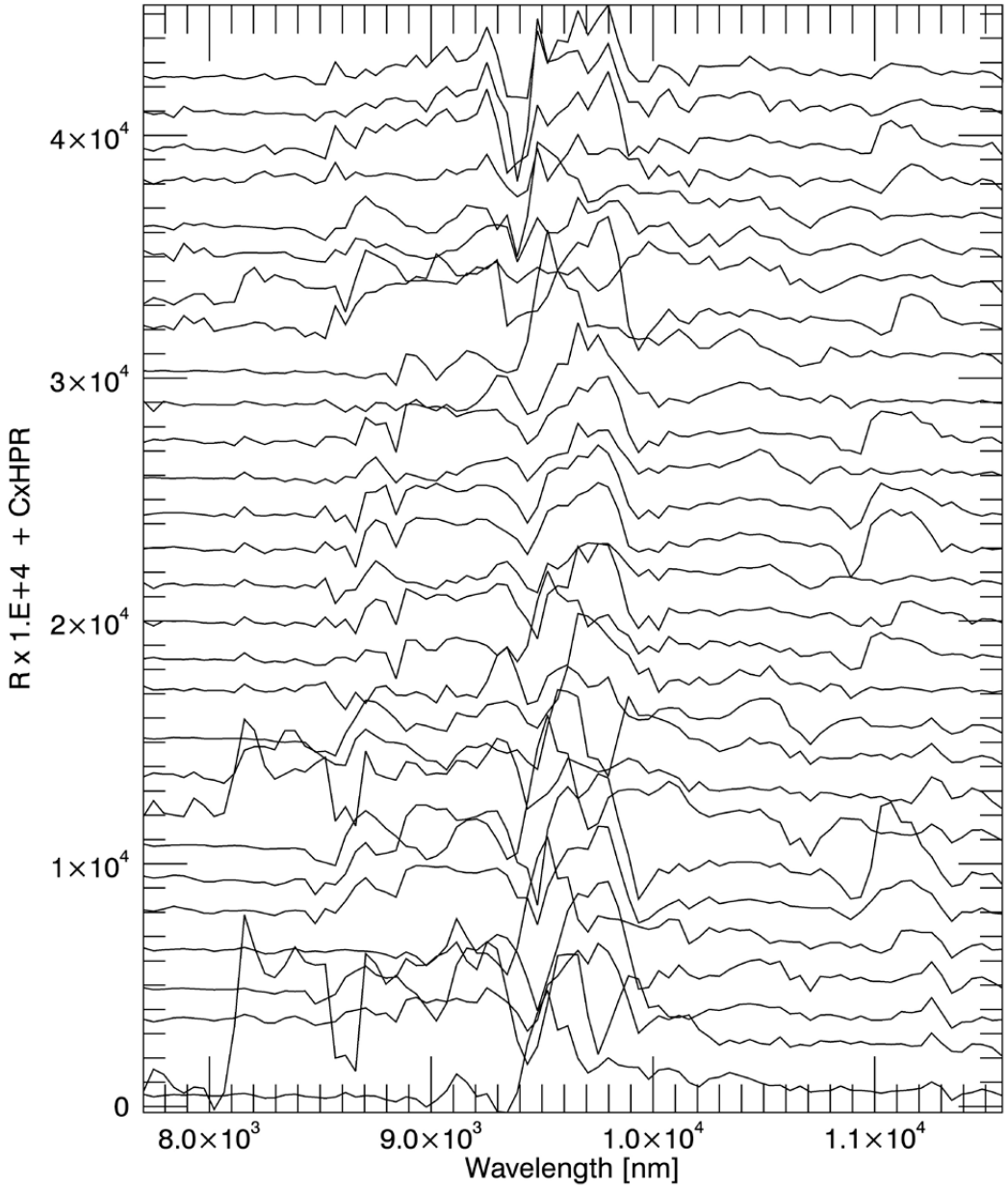

Fig. 3. The LWIR reflectance mean spectra of all 29 ROIs of the Kemi samples after the high-pass component (f = 100.) has been added to the spectra. The curves are vertically shifted for clarity.

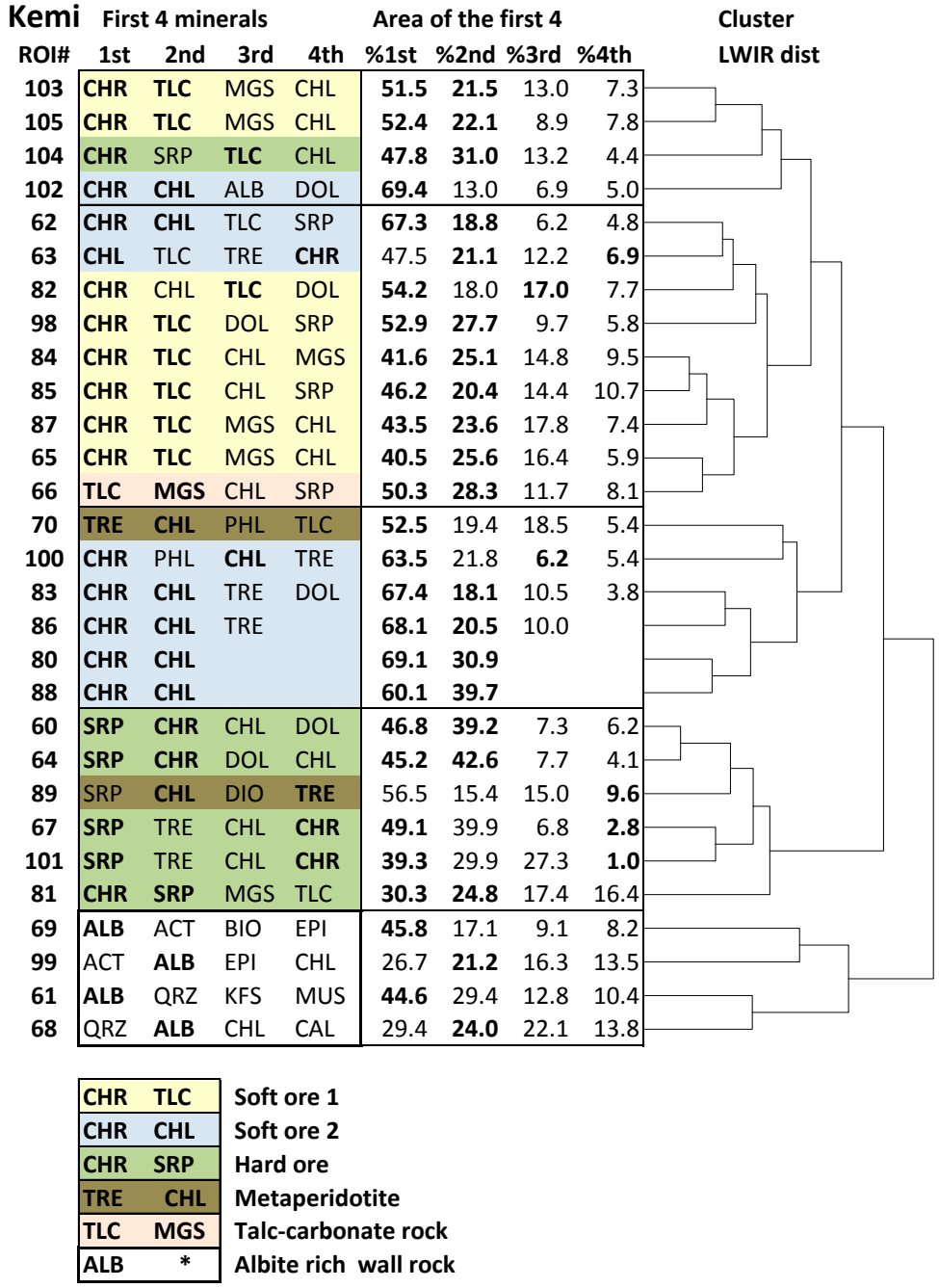

Kemi	First 4 minerals				Area of the first 4				Cluster
ROI#	1st	2nd	3rd	4th	%1st	%2nd	%3rd	%4th	LWIR dist
103	CHR	TLC	MGS	CHL	51.5	21.5	13.0	7.3	
105	CHR	TLC	MGS	CHL	52.4	22.1	8.9	7.8	
104	CHR	SRP	TLC	CHL	47.8	31.0	13.2	4.4	
102	CHR	CHL	ALB	DOL	69.4	13.0	6.9	5.0	
62	CHR	CHL	TLC	SRP	67.3	18.8	6.2	4.8	
63	CHL	TLC	TRE	CHR	47.5	21.1	12.2	6.9	
82	CHR	CHL	TLC	DOL	54.2	18.0	17.0	7.7	
98	CHR	TLC	DOL	SRP	52.9	27.7	9.7	5.8	
84	CHR	TLC	CHL	MGS	41.6	25.1	14.8	9.5	
85	CHR	TLC	CHL	SRP	46.2	20.4	14.4	10.7	
87	CHR	TLC	MGS	CHL	43.5	23.6	17.8	7.4	
65	CHR	TLC	MGS	CHL	40.5	25.6	16.4	5.9	
66	TLC	MGS	CHL	SRP	50.3	28.3	11.7	8.1	
70	TRE	CHL	PHL	TLC	52.5	19.4	18.5	5.4	
100	CHR	PHL	CHL	TRE	63.5	21.8	6.2	5.4	
83	CHR	CHL	TRE	DOL	67.4	18.1	10.5	3.8	
86	CHR	CHL	TRE		68.1	20.5	10.0		
80	CHR	CHL			69.1	30.9			
88	CHR	CHL			60.1	39.7			
60	SRP	CHR	CHL	DOL	46.8	39.2	7.3	6.2	
64	SRP	CHR	DOL	CHL	45.2	42.6	7.7	4.1	
89	SRP	CHL	DIO	TRE	56.5	15.4	15.0	9.6	
67	SRP	TRE	CHL	CHR	49.1	39.9	6.8	2.8	
101	SRP	TRE	CHL	CHR	39.3	29.9	27.3	1.0	
81	CHR	SRP	MGS	TLC	30.3	24.8	17.4	16.4	
69	ALB	ACT	BIO	EPI	45.8	17.1	9.1	8.2	
99	ACT	ALB	EPI	CHL	26.7	21.2	16.3	13.5	
61	ALB	QRZ	KFS	MUS	44.6	29.4	12.8	10.4	
68	QRZ	ALB	CHL	CAL	29.4	24.0	22.1	13.8	

CHR	TLC	Soft ore 1
CHR	CHL	Soft ore 2
CHR	SRP	Hard ore
TRE	CHL	Metaperidotite
TLC	MGS	Talc-carbonate rock
ALB	*	Albite rich wall rock

Fig. 4. A dendrogram illustration for a classification of the LWIR mean spectra of the samples from the Kemi mine. The Cr ore is separated into chromite-talc (yellow), chromite-chlorite (blue) and chromite-serpentine (green). Different types of wall rocks and ores are separated, with a few exceptions.

Quantitative mineralogical prediction from the mean spectra of the SisuROCK Kemi data

The quantitative mineral content for each sample from the Kemi mine was predicted from the filtered (f = 100.) LWIR mean spectra using the PLS regression model. The total number of samples with ROIs from Kemi was 29. The regression model for each sample in turn was built of the other 28 sample spectra.

The PLSR prediction for the main minerals produced the following accuracy parameters shown in Table 1. The classical linear unmixing (UMXR) method produced quite similar values for the error parameters as the PLSR. The simultaneous high correlation coefficient and the low p-value in Table 1 suggest that the mean absolute estimation errors (MAEs) are reliable (low p-values and moderate CCs) for actinolite, albite, chromite, dolomite, magnesite, quartz, serpentine, talc and tremolite. These well-predicted minerals cover 2744 area

units from the total 2888 au. Figure 5 shows that if the sum area [au] for a mineral is very small, it will produce a low reliability (high p-value), and vice versa. In this case, the low CC and high p-value have dropped chlorite and phlogopite from the list of the expected best success; the reason for this is discussed later in this paper. This list of well-quantified minerals essentially covers those materials that classify the ore types and the wall rocks in this sample set from the Kemi mine.

The same statistics were also computed for all Kemi ROIs (Table 2 and examples in Fig. 6, where the key to the mineral index (numbers) is in Table 1 in the two first columns). According to the correlation coefficient and the p-value, only two ROIs from 29 have unreliable estimates. They are numbers 68 and 99 (Table 2). The reason for their failure is that their mineralogy is 'strange', i.e. they do not have analogous samples among the modelling group. All other 27 ROIs obtained reliable

Kemi ROI prediction

ROI NO	PLS MAE%	PLS RMSE%	PLS CC	Predictv Minerals	S-area	p-value
60	1.58	3.05	0.99	19	100.00	0.0000
61	14.78	20.71	0.74	19	98.82	0.0003
62	2.90	3.55	0.98	19	99.98	0.0000
63	5.94	10.16	0.66	19	99.43	0.0022
64	1.16	1.82	0.99	19	99.98	0.0000
65	2.32	3.90	0.96	19	100.00	0.0000
66	3.77	7.43	0.87	19	99.93	0.0000
67	2.61	4.06	0.96	19	99.50	0.0000
68	8.76	13.15	0.18	19	99.44	0.4690
69	5.85	9.24	0.59	19	96.88	0.0078
70	5.08	9.25	0.68	19	99.79	0.0013
80	2.38	4.30	0.99	19	99.98	0.0000
81	2.46	3.80	0.95	19	99.99	0.0000
82	1.62	2.18	0.99	19	99.99	0.0000
83	1.85	2.85	0.99	19	99.78	0.0000
84	2.42	5.29	0.97	19	100.00	0.0000
85	1.23	1.73	0.99	19	100.00	0.0000
86	2.62	4.22	0.97	19	99.66	0.0000
87	2.40	4.31	0.94	19	99.99	0.0000
88	2.94	5.46	0.96	19	99.92	0.0000
89	5.66	10.58	0.73	19	98.10	0.0004
98	2.14	2.60	0.99	19	100.00	0.0000
99	6.53	8.80	0.34	19	98.31	0.1602
100	4.24	7.98	0.85	19	99.92	0.0000
101	4.28	7.47	0.79	19	98.40	0.0000
102	3.10	4.90	0.95	19	99.93	0.0000
103	2.08	2.94	0.99	19	99.99	0.0000
104	5.06	8.26	0.76	19	100.00	0.0001
105	1.86	3.20	0.97	19	100.00	0.0000
Total area [au]					**2887.71**	

Table 2. The statistical descriptors for the region of interest (ROI) prediction by partial least squares regression (PLSR) in the Kemi case. There are only two ROIs (unbolded, 68 and 99) for which the estimates and the error measures are not acceptable. The reason for this is that the quantities of the rare minerals are naturally small and they do not greatly affect the measures in the majority of the samples. The main minerals are naturally promptly represented by the area and the spectra.

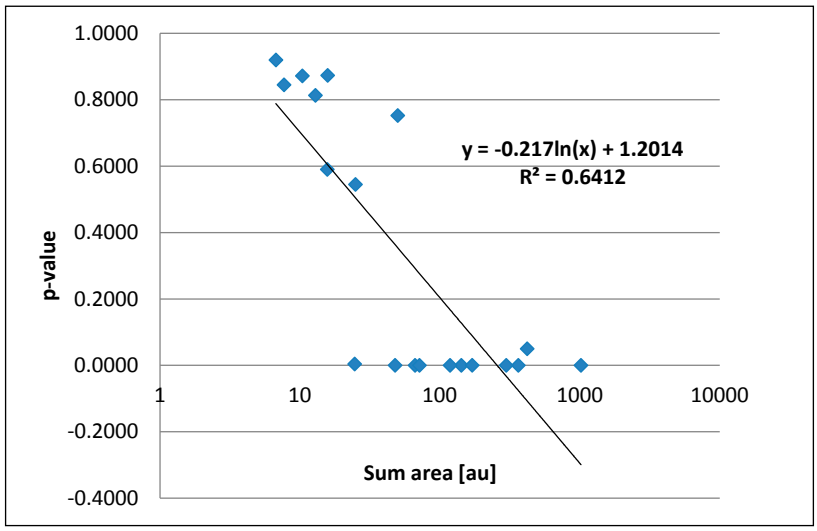

Fig. 5. The total mineral area and the risk measure p-values are logarithmically related, i.e. they are inversely proportional in the Kemi LWIR case.

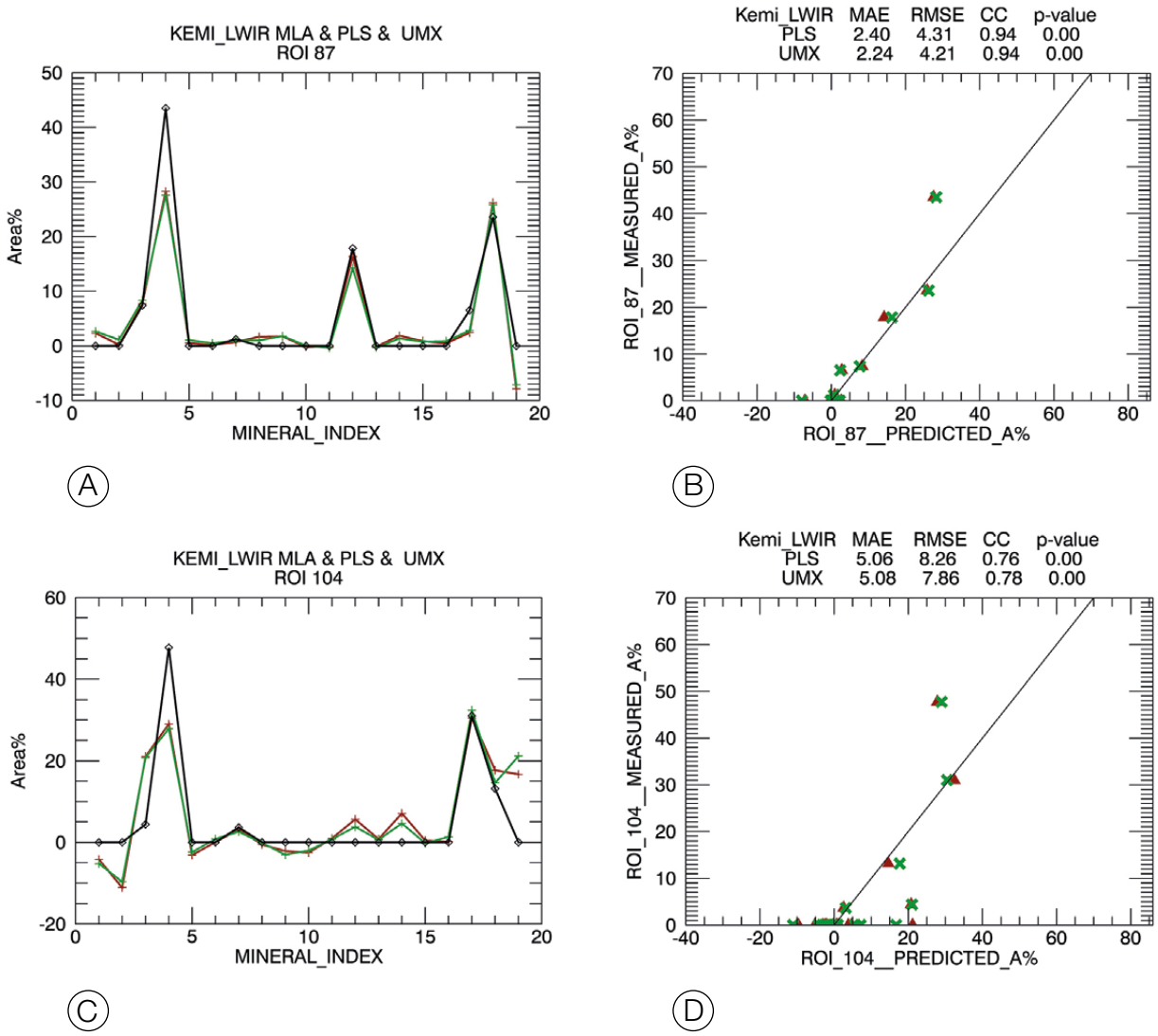

Fig. 6. Examples of the ROI prediction for the Kemi data. On the left (A and C): partial least squares estimates (PLS, red) and unmixing estimates (UMX, green) prediction from the LWIR data for the mineral contents of two Kemi ROIs, nos. 87 and 104). The measured quantities are shown by the black line. The mineral index is on the x-axis; see the respective mineral names in Table 1, the two first columns. On the right (B and D): The scatter diagrams between the predicted and the measured mineral quantities of the same ROIs. All ROI data were computed this way; the resulting statistics are presented in Table 2. In the upper figures (A and B), the dominant minerals are chlorite, chromite, magnesite and talc; and in the lower pictures (C and D) the peaks are chlorite, chromite, dolomite, serpentine and talc. Enhancement of the high-pass component (f=100.) was used for the prediction. UMX and PLS are indicated in green and red, respectively.

estimates. The quantities of the rare mineral grains are, by definition, very small and they cannot greatly affect the statistical measures, i.e. the predictions and the MLA reference quantities of the rare minerals are close to zero.

In Figure 6, the PLSR result is first printed by a red symbol and thereafter the UMX result by a green symbol. If both red and green are seen in the figures, the results are different, but if only a green colour occurs, the results coincide. In Figure 6, B and D, statistical errors and correlations and other parameters for both methods are presented on top of the diagram. Because two main minerals, namely chromite and chlorite, received only modest MAEs (Table 1), either the samples did not cover their mineralogical variation or their LWIR spectra were not unique enough to be better distinguished from the background. Concerning all mineral predictions in the Kemi case, PLSR and UMXR produced statistically very coincident results: It cannot be said which one performs better.

Quantitative mineralogical prediction from the Kemi LWIR pixel images

The LWIR SisuROCK image pixels of the Kemi samples were also interpreted for the mineral quantities using PLSR estimation. Before this, the image was still filtered by a 3-term median (Råde and Westergren 2004) along the image lines in order to avoid noise. In addition to the 29 mean spectra, the regression model was complemented with the spectra of 19 single minerals. This is necessary, because a pixel in the LWIR image may be occupied by a single mineral. All together, 48 LWIR spectra were used for the mod-

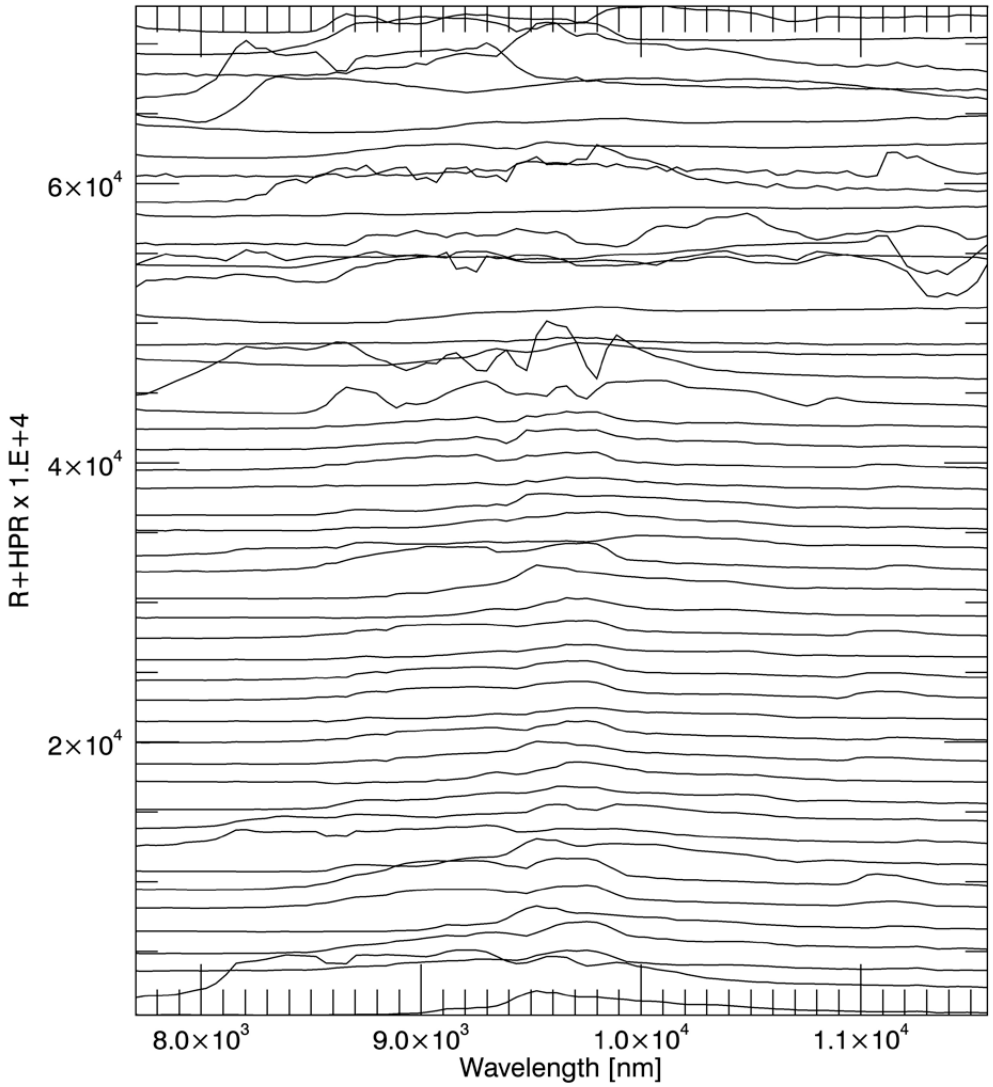

Fig. 7. The ROI and the single mineral LWIR mean spectra for the Kemi case. The ROI spectra were used for estimating quantities from the mean spectra and all were used for the estimation of mineral quantities from the Kemi pixel images. The high-pass component (f = 0.2) was not added to the original spectra. All spectra are shifted vertically for clarity.

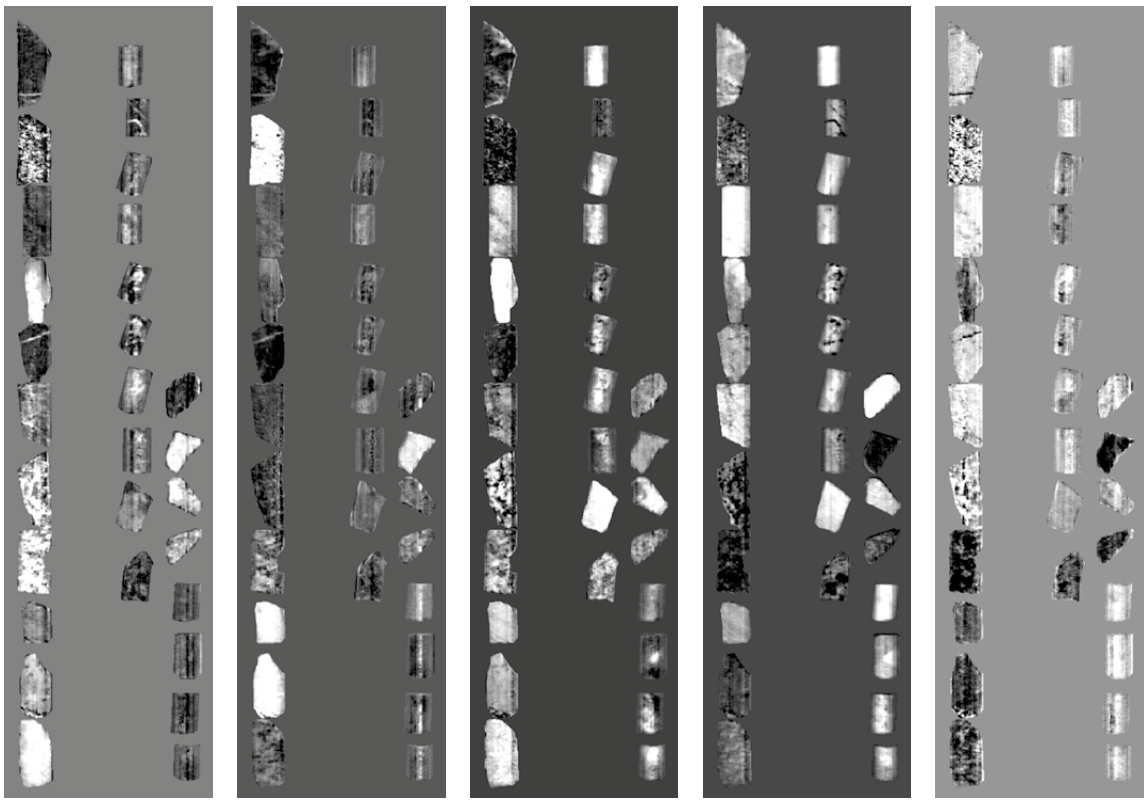

Actinolite Albite Chlorite Chromite Dolomite

Fig. 8. Illustration of the PLSR for the first five main minerals/pixel estimates about the Kemi case. The greytone variation limits from black to white for the minerals are: Actinolite 0.0-46.1%, Albite 0.0-56.8%, Chlorite, 0.0-79.5%, Chromite 0.0-100.0% and Dolomite 0.0-42.1%.

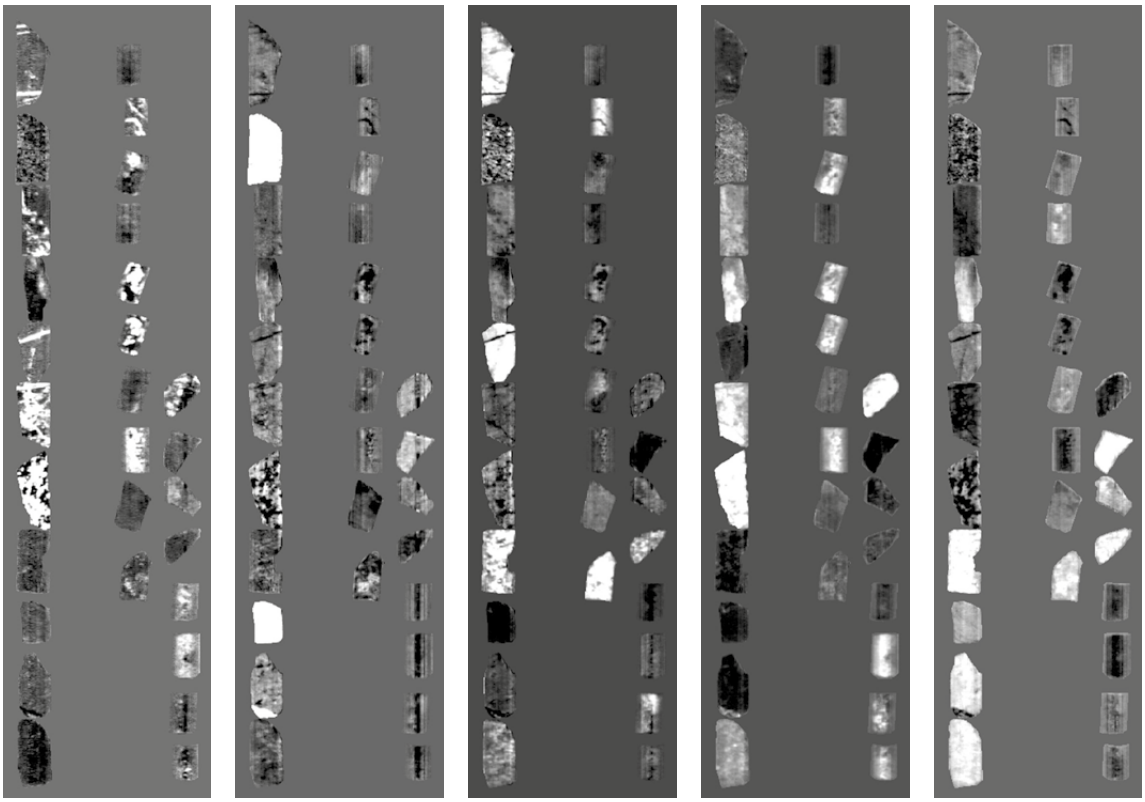

Magnesite Quartz Serpentine Talc Tremolite

Fig. 9. Illustration of the PLSR for the last five main minerals/pixel estimates about the Kemi case. The greytone variation limits from black to white for the minerals are: Magnesite 0.0-100.0%, Quartz 0.0-100.0%, Serpentine 0.0-100.0%, Talc 0.0-81.0% and Tremolite 0.0-41.2%.

elling. Their spectra are shown in their original form in Figure 7, which presents all ROI and mineral spectra that were used for this purpose. The high-pass multiplier was not used (i.e. f = 0.) for the pixel prediction, because the pixel spectra are noisier than the mean spectra. The additional spectra were those for actinolite, albite, chlorite, chromite, biotite, calcite, dolomite, diopside, epidote, hornblende, K-feldspar, magnesite, muscovite, phlogopite, plagioclase, quartz, serpentine, talc and tremolite. The result from the pixel image interpretation is expected to have a slightly lower level of accuracy than in the previous chapter for the mean spectra. The images for the predicted main minerals are presented in Figures 8 and 9.

Mineralogical clusters of the Pyhäsalmi and Kedonojankulma samples from MLA

The frequent minerals encountered in the MLA studies of the ***Pyhäsalmi*** samples related to the alteration study were (from the most common to rarest): quartz, cordierite, plagioclase, biotite, muscovite, phlogopite, pinite, pyrite, chlorite, gedrite, pyrrhotite, sillimanite, anthophyllite, talc, muscovite-chlorite mix, sphalerite and Fe oxide-mica mix. The remaining minerals covered less than 1% of the total 'surface' analysed: They were ilmenite, magnetite, apatite, kaolinite, almandine, albite, chalcopyrite, ferrogedrite, rutile, K-feldspar, calcite, an unclassified mineral, illite, gahnite, monazite-(Ce), allanite, zircon and galena.

The frequent minerals encountered in the MLA studies of the ***Kedonojankulma*** samples related to the alteration study were (from the most common to rarest): albite, quartz, K-feldspar, muscovite, chlorite, laumontite, calcite, plagioclase, allanite, chalcopyrite, epidote and illite. The remaining minerals covered less than 1% of the total 'surface' analysed: They were titanite, hornblende, biotite, pyrite, apatite, arsenopyrite, tourmaline, pyrrhotite, rutile, kaolinite, tetrahedrite, actinolite, an unclassified mineral, zircon, ilmenite, sphalerite, fluorite, britholite, scheelite, thorite, galena, claushalite(PbSe), cobaltite and silver. Table 3, column 'S-area', presents the frequency of different minerals exposed to the MLA measurements in the combined Pyhäsalmi-Kedonojankulma study.

The MLA data from the combined sample set were unsupervisedly clustered. The dendrogram (Fig. 10) shows the internal pattern of hierarchy of the mineralogical contents. The samples from the Pyhäsalmi and Kedonojankulma locate in different clusters, except for some extreme cases.

PYS-Kedo	First 4 minerals				Area of the first 4				Cluster
ROI#	1st	2nd	3rd	4th	%1st	%2nd	%3rd	%4th	MLA dist
111	PHL	QRZ	CRD	PLG	38.0	18.2	14.5	7.8	
112	CRD	MUS	QRZ	PLG	28.6	23.0	18.0	16.4	
110	QRZ	CRD	PLG	SIL	60.1	29.0	3.5	2.1	
120	QRZ	BIO	CRD	MUS	67.1	14.1	13.0	2.5	
118	QRZ	CRD	BIO	GED	46.3	23.8	21.9	2.4	
119	QRZ	CRD	BIO	CHL	56.8	21.3	17.4	2.2	
108	QRZ	CRD	BIO	MUS	41.8	24.7	14.0	10.8	
116	QRZ	PLG	MUS	BIO	51.5	21.1	12.3	9.2	
117	QRZ	MUS	PLG	BIO	59.3	15.4	9.2	6.2	
114	QRZ	PHL	CRD	PIN	51.0	15.0	13.2	9.6	
115	QRZ	PHL	BIO	CHL	55.1	34.2	8.9	1.5	
149	QRZ	ALB	CHL	KFS	99.8	0.1	0.1	0.0	
125	ALB	QRZ	KFS	CHL	30.7	21.1	14.0	10.4	
150	ALB	KFS	QRZ	CHL	33.5	19.2	11.8	11.5	
132	ALB	KFS	MUS	QRZ	31.1	24.7	17.1	10.8	
138	ALB	QRZ	KFS	CHL	39.2	28.3	18.3	5.0	
152	ALB	QRZ	KFS	CHL	39.7	30.1	16.2	7.9	
140	ALB	QRZ	KFS	CHL	35.6	30.4	17.5	6.6	
136	ALB	QRZ	KFS	CHL	38.4	27.3	16.6	4.0	
146	ALB	QRZ	KFS	CHL	39.6	34.8	15.0	5.6	
134	ALB	KFS	QRZ	CHL	43.7	24.9	23.4	3.7	
147	ALB	QRZ	KFS	CHL	39.6	25.7	23.5	5.1	
128	ALB	QRZ	KFS	PLG	34.2	30.7	12.8	8.8	
130	QRZ	KFS	ALB	CHL	31.4	30.8	28.4	4.2	
153	QRZ	ALB	KFS	CHL	35.2	30.6	26.5	4.0	
126	KFS	ALB	QRZ	CHP	40.9	30.3	14.2	4.2	
142	ALB	KFS	CHL	QRZ	71.0	13.0	6.8	3.2	
144	ALB	QRZ	KFS	CHL	51.9	16.5	13.1	9.7	
94	ALB	MUS	KFS	QRZ	53.3	21.8	11.3	9.4	
97	ALB	LAU	MUS	KFS	35.6	20.2	12.2	7.8	
121	PLG	BIO	QRZ	PRH	56.7	22.7	18.2	1.0	
122	PLG	QRZ	GED	BIO	55.7	17.3	8.1	5.3	
109	PLG	BIO	QRZ	CRD	32.9	29.3	16.5	4.9	
113	MUS	PYR	QRZ	SPH	64.1	11.6	9.9	4.1	
123	MUS	QRZ	KFS	CHP	56.0	25.3	13.2	3.8	
92	LAU	CAL	ALL	ILL	41.6	40.5	7.4	3.4	

Fig. 10. Dendrogram of the mineralogy (MLA data) for the Pyhäsalmi and Kedonojankulma samples clustered unsupervisedly using the Euclidean distance method. The four first most abundant minerals are indicated by their acronyms (after the ROI#) on the left and their respective mineral quantities [area %] by the numbers on the right. The dendrogram shows the mineralogical pattern of hierarchy for both test sites. The acronyms are: ALB = albite, ALL = allanite, BIO = biotite, CAL = calcite, CHP = chalcopyrite, CHL = chlorite, CRD = cordierite, GED = gedrite, ILL = illite, KFS = K-feldspar, LAU = laumontite, MUS = muscovite, PHL = phlogopite, PIN = pinite, PLG = plagioclase, PYR = pyrite, QRZ = quartz, SIL = sillimanite, SPH = sphalerite.

Contribution of the SisuROCK LWIR assays to the estimation of mineral quantities of the Pyhäsalmi – Kedonojankulma samples

Apparent mineralogical clusters from the Pyhäsalmi – Kedonojankulma LWIR mean spectra

The LWIR mean spectra from the combined sample set were also clustered using the high-pass enhanced (f = 100.) mean spectra. The hierarchy of the LWIR data of the Pyhäsalmi and Kedonojankulma samples is illustrated by Figure 11. When comparing this with the previous dendrogram (Fig. 10), the samples from different sites still locate in separate clusters, but there are exceptions. The internal hierarchy of the samples is approximately the same in both diagrams; only the order of the clusters may differ.

PYS-Kedo	First 4 minerals				Area of the first 4				Cluster
ROI#	1st	2nd	3rd	4th	%1st	%2nd	%3rd	%4th	LWIR dist
109	PLG	BIO	QRZ	CRD	32.9	29.3	16.5	4.9	
111	PHL	QRZ	CRD	PLG	38.0	18.2	14.5	7.8	
121	PLG	BIO	QRZ	PRH	56.7	22.7	18.2	1.0	
122	PLG	QRZ	GED	BIO	55.7	17.3	8.1	5.3	
152	ALB	QRZ	KFS	CHL	39.7	30.1	16.2	7.9	
112	CRD	MUS	QRZ	PLG	28.6	23.0	18.0	16.4	
134	ALB	KFS	QRZ	CHL	43.7	24.9	23.4	3.7	
153	QRZ	ALB	KFS	CHL	35.2	30.6	26.5	4.0	
130	QRZ	KFS	ALB	CHL	31.4	30.8	28.4	4.2	
113	MUS	PYR	QRZ	SPH	64.1	11.6	9.9	4.1	
144	ALB	QRZ	KFS	CHL	51.9	16.5	13.1	9.7	
150	ALB	KFS	QRZ	CHL	33.5	19.2	11.8	11.5	
140	ALB	QRZ	KFS	CHL	35.6	30.4	17.5	6.6	
147	ALB	QRZ	KFS	CHL	39.6	25.7	23.5	5.1	
142	ALB	KFS	CHL	QRZ	71.0	13.0	6.8	3.2	
92	LAU	CAL	ALL	ILL	41.6	40.5	7.4	3.4	
136	ALB	QRZ	KFS	CHL	38.4	27.3	16.6	4.0	
146	ALB	QRZ	KFS	CHL	39.6	34.8	15.0	5.6	
128	ALB	QRZ	KFS	PLG	34.2	30.7	12.8	8.8	
138	ALB	QRZ	KFS	CHL	39.2	28.3	18.3	5.0	
126	KFS	ALB	QRZ	CHP	40.9	30.3	14.2	4.2	
132	ALB	KFS	MUS	QRZ	31.1	24.7	17.1	10.8	
125	ALB	QRZ	KFS	CHL	30.7	21.1	14.0	10.4	
123	MUS	QRZ	KFS	CHP	56.0	25.3	13.2	3.8	
94	ALB	MUS	KFS	QRZ	53.3	21.8	11.3	9.4	
97	ALB	LAU	MUS	KFS	35.6	20.2	12.2	7.8	
118	QRZ	CRD	BIO	GED	46.3	23.8	21.9	2.4	
119	QRZ	CRD	BIO	CHL	56.8	21.3	17.4	2.2	
120	QRZ	BIO	CRD	MUS	67.1	14.1	13.0	2.5	
110	QRZ	CRD	PLG	SIL	60.1	29.0	3.5	2.1	
108	QRZ	CRD	BIO	MUS	41.8	24.7	14.0	10.8	
114	QRZ	PHL	CRD	PIN	51.0	15.0	13.2	9.6	
116	QRZ	PLG	MUS	BIO	51.5	21.1	12.3	9.2	
115	QRZ	PHL	BIO	CHL	55.1	34.2	8.9	1.5	
117	QRZ	MUS	PLG	BIO	59.3	15.4	9.2	6.2	
149	QRZ	ALB	CHL	KFS	99.8	0.1	0.1	0.0	

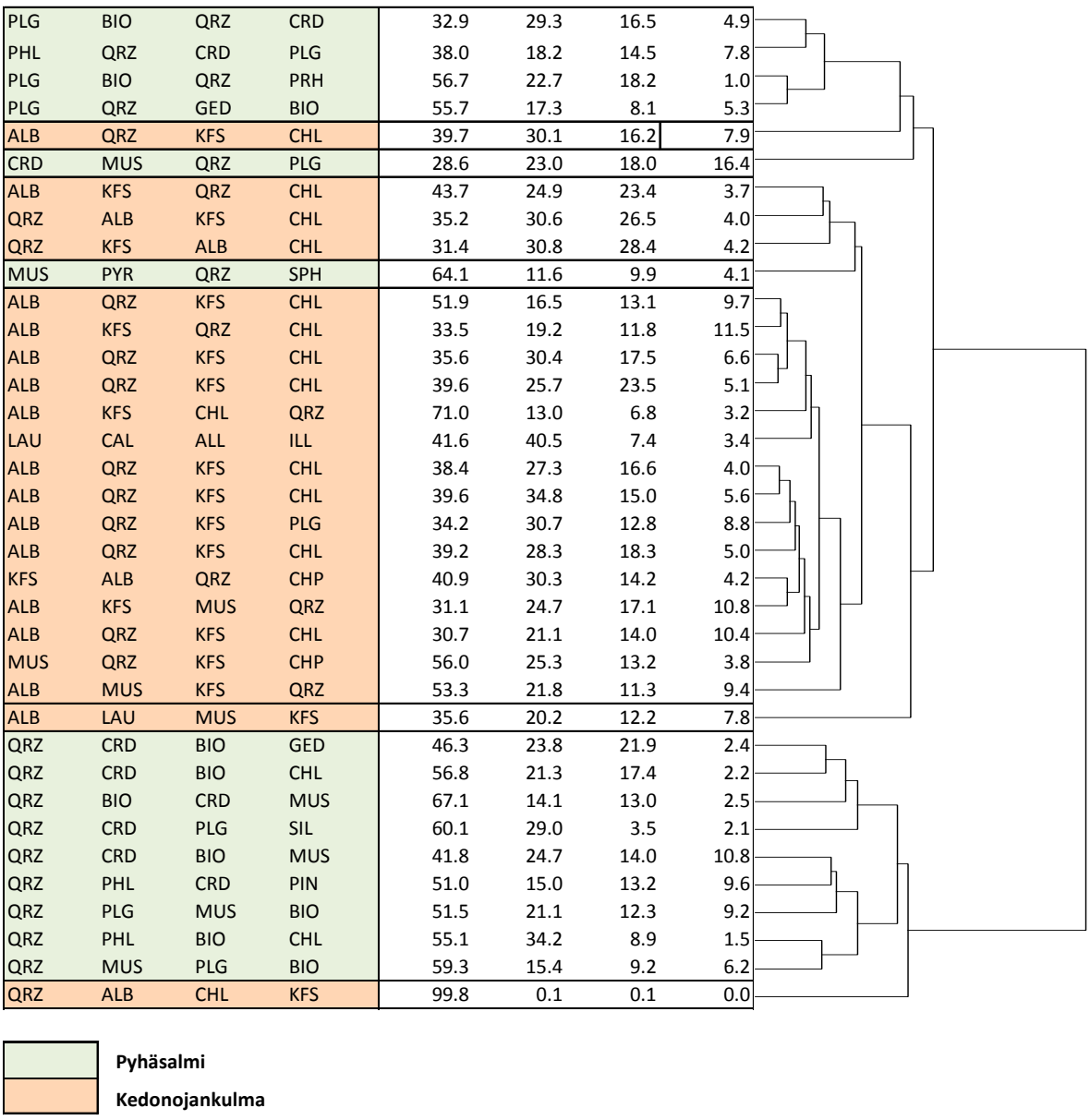

Fig. 11. Dendrogram of the LWIR spectra for the Pyhäsalmi and Kedonojankulma samples clustered unsupervisedly. The four first most abundant minerals are indicated by their acronyms (after the ROI#) on the left and their respective mineral quantities [%] by the numbers on the right. The dendrogram shows the LWIR-based pattern of hierarchy for both test sites. The mineralogical pattern and the LWIR pattern are very similar (cf. Fig. 16).

Quantitative mineralogical prediction from the mean spectra of the SisuROCK Pyhäsalmi and Kedonojankulma LWIR data

The quantitative mineral content of the Pyhäsalmi and Kedonojankulma samples was predicted using the PLS regression model on the mean spectra. The model was built for each sample from the other 35 samples out of the 36 in total. The union coverage of all the 36 samples was 3600 au (± a small area error in the MLA assays).

The predictions for the minerals produced quantity estimates, for which the respective error and reliability measures are presented in Table 3. The well-quantified minerals (bolded in Table 3) essentially cover those minerals that classify the alteration type and intensity and the wall rocks in this Pyhäsalmi and Kedonojankulma sample set. This prediction was also computed for the ROIs of the samples (Table 4). A predicted ROI (a row in Table 4) means (a predicted mineral composition and) the reliability measures for a sample.

Pyhäsalmi_Kedonojankulma mineral prediction

Mineral index	Mineral	PLS MAE%	PLS RMSE%	PLS CC	Predictv ROIs	S-area [au]	p-value
1	Actinolite	0.25	0.30	-0.02	35	0.73	0.9064
2	**Albite**	**15.75**	**21.56**	**0.56**	**35**	**711.27**	**0.0004**
3	**Allanite**	**0.94**	**1.30**	**0.63**	**35**	**28.14**	**0.0000**
4	Almandine	0.08	0.12	0.04	35	0.86	0.8011
5	Anthophyllite	0.98	1.37	0.10	35	8.44	0.5675
6	Apatite	0.10	0.12	0.19	35	3.84	0.2735
7	Arsenopyrite	0.09	0.14	-0.02	35	0.66	0.9208
8	**Biotite**	**5.57**	**8.22**	**0.45**	**35**	**166.77**	**0.0059**
9	Calcite	5.14	9.77	0.03	35	47.89	0.8465
10	**Chalcopyrite**	**0.86**	**1.21**	**0.34**	**35**	**17.15**	**0.0439**
11	Chlorite	4.27	5.85	0.21	35	119.22	0.2300
12	**Cordierite**	**1.97**	**2.80**	**0.95**	**35**	**182.27**	**0.0000**
13	Epidote	1.33	1.76	0.21	35	22.62	0.2180
14	Fe_oxide	0.04	0.06	0.05	35	0.32	0.7659
15	Feox_mica_mix	0.45	0.69	0.00	35	2.75	0.9959
16	Gedrite	1.89	2.73	0.05	35	14.53	0.7524
17	Hornblende	3.19	3.87	-0.02	35	9.54	0.9028
18	Illite	0.96	1.53	0.16	35	22.06	0.3502
19	**Ilmenite**	**0.14**	**0.18**	**0.53**	**35**	**2.23**	**0.0010**
20	**K_feldspar**	**8.02**	**10.11**	**0.67**	**35**	**362.60**	**0.0000**
21	Kaolinite	0.13	0.21	-0.12	35	2.08	0.4760
22	**Laumontite**	**4.44**	**8.04**	**0.42**	**35**	**62.92**	**0.0109**
23	Magnetite	0.36	0.52	-0.15	35	2.90	0.3928
24	**Muscovite_Chlorite_mix**	**0.34**	**0.47**	**0.41**	**35**	**7.26**	**0.0122**
25	**Muscovite**	**5.97**	**8.47**	**0.81**	**35**	**279.13**	**0.0000**
26	**Phlogopite**	**5.22**	**7.65**	**0.55**	**35**	**89.12**	**0.0005**
27	Pinite	1.89	2.66	0.22	35	31.36	0.1951
28	**Plagioclase**	**6.96**	**9.42**	**0.78**	**35**	**244.06**	**0.0000**
29	Pyrite	1.64	2.54	0.13	35	23.59	0.4432
30	Pyrrhotite	1.00	1.62	-0.07	35	13.36	0.6903
31	**Quartz**	**5.96**	**7.88**	**0.94**	**35**	**1100.71**	**0.0000**
32	Rutile	0.06	0.07	0.01	35	0.90	0.9473
33	Sillimanite	0.62	1.02	0.18	35	8.81	0.2875
34	Sphalerite	0.54	0.87	0.01	35	4.43	0.9575
35	Talc	1.15	1.93	-0.03	35	7.56	0.8608
36	Tetrahedrite	0.09	0.14	-0.01	35	0.50	0.9653
37	Titanite	0.80	1.06	0.21	35	10.44	0.2099
38	Tourmaline	0.08	0.15	-0.63	35	1.08	0.0000
39	Unclassified	0.03	0.04	-0.04	35	0.67	0.8324
40	Zircon	0.01	0.02	0.10	35	0.29	0.5654
	Total area [au]					**3615.04**	

Table 3. Statistics showing the success or failure of the mineral prediction by partial least squares regression (PLSR) concerning the LWIR spectra of the Pyhäsalmi and Kedonojankulma samples. Generally, those minerals that are abundant are more successfully estimated.

Pyhäsalmi-Kedonojankulma ROI prediction

ROI NO	PLS MAE%	PLS RMSE%	PLS CC	Predictv Minerals	S-area	p-value
92	5.61	12.83	0.00	40	100.00	0.9851
94	2.53	5.64	0.79	40	100.00	0.0000
97	5.88	13.19	-0.07	40	100.00	0.6553
108	1.74	3.16	0.92	40	100.50	0.0000
109	3.89	7.80	0.43	40	100.05	0.0060
110	3.53	7.31	0.81	40	100.08	0.0000
111	3.68	7.33	0.52	40	100.36	0.0006
112	3.41	6.42	0.63	40	100.24	0.0000
113	3.85	7.20	0.73	40	100.35	0.0000
114	2.94	5.46	0.81	40	100.77	0.0000
115	1.89	3.05	0.95	40	100.00	0.0000
116	2.32	5.10	0.82	40	101.32	0.0000
117	1.57	2.57	0.98	40	101.53	0.0000
118	1.60	2.70	0.95	40	100.14	0.0000
119	1.26	2.36	0.98	40	100.31	0.0000
120	2.03	5.43	0.90	40	101.19	0.0000
121	2.12	3.93	0.93	40	100.01	0.0000
122	1.96	3.99	0.94	40	100.34	0.0000
123	1.99	4.46	0.90	40	103.79	0.0000
125	1.03	1.87	0.96	40	100.08	0.0000
126	1.76	4.38	0.84	40	100.01	0.0000
128	1.36	2.65	0.94	40	100.57	0.0000
130	2.26	5.50	0.98	40	100.20	0.0000
132	1.14	2.17	0.97	40	101.60	0.0000
134	1.38	2.86	0.97	40	100.07	0.0000
136	1.15	2.34	0.97	40	99.90	0.0000
138	1.26	2.23	0.96	40	100.17	0.0000
140	1.25	2.68	0.98	40	100.63	0.0000
142	1.55	3.19	0.96	40	100.04	0.0000
144	1.61	4.57	0.91	40	100.01	0.0000
146	0.60	1.23	0.99	40	99.94	0.0000
147	0.84	1.43	0.99	40	100.29	0.0000
149	4.48	9.38	0.88	40	100.00	0.0000
150	1.27	2.42	0.94	40	100.03	0.0000
152	2.49	5.21	0.92	40	100.36	0.0000
153	1.17	2.16	0.97	40	100.18	0.0000
Total area [au]					**3615.06**	

Table 4. The statistical descriptors for the region of interest (ROI) prediction by partial least squares regression (PLSR) in the Pyhäsalmi-Kedonojankulma case. Here, too, there are only two ROIs (92 and 97), for which the estimates and the error measures are not acceptable. The remaining 34 ROIs are acceptable.

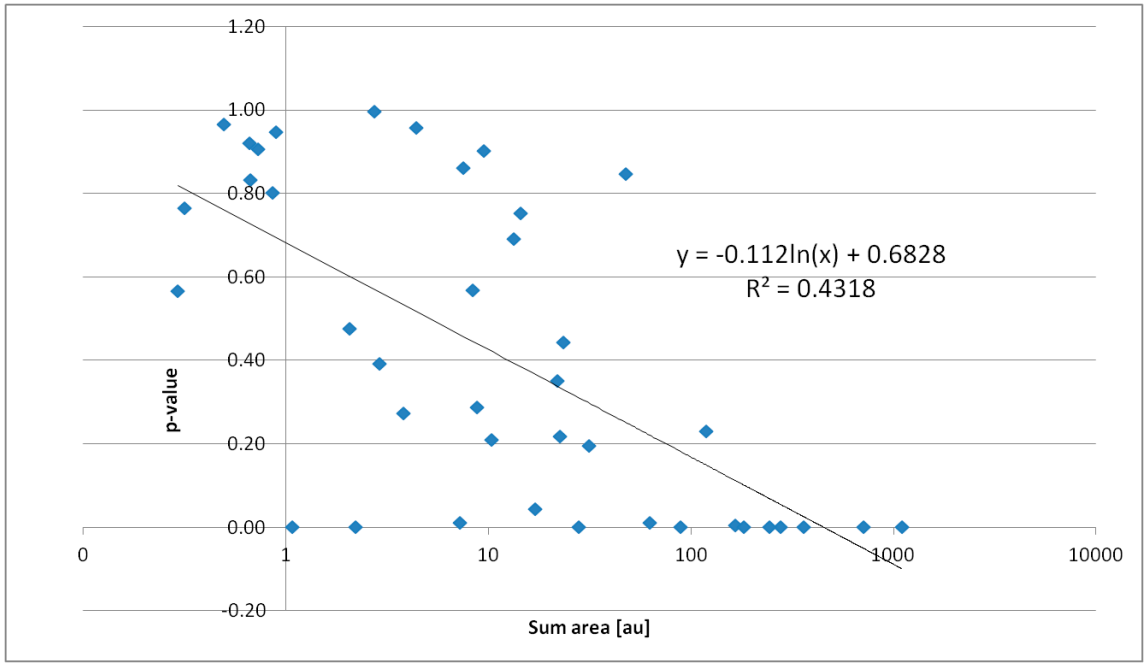

Fig. 12. In the Pyhäsalmi-Kedonojankulma case, the p-value is inversely proportional to the logarithm of the sum area exposed to the sensor.

The graph in Figure 12 shows the relationship between the sum area and the p-value: if the sum area for a mineral is small, it tends to produce a high p-value (and small CC). Albite, allanite, biotite, chalcopyrite, cordierite, K-feldspar, laumontite, muscovite, phlogopite, plagioclase and quartz are more reliably quantified than the rest of the minerals (Table 3). However, although chlorite occurs in many samples (total 421 au), it drops out from the list of well-predicted minerals. The well-predicted minerals comprise 3254 au from the total 3615 au. The 34 ROIs from total of 36 are predicted reliably, as can be seen in Table 4. It is again emphasized that this result concerns only those regression models that were constructed here based on the LWIR spectra of the 35 other samples for each one in turn out of the total of 36 samples. Concerning all mineral prediction in the Pyhäsalmi-Kedonojankulma case, the PLRS and UMXR produced statistically very similar results.

Quantitative mineralogical prediction from the SisuROCK the LWIR images of the Pyhäsalmi and Kedonojankulma samples

The estimation in this section is targeted at single pixels of the Pyhäsalmi and Kedonojankulma SisuROCK LWIR image. Before this, the image was filtered by a 3-term median (Råde and Westergren 2004) along the image lines in order to avoid noise.

This PLS Regression model was built and computed, in addition to the mean sample spectra, by also using the 18 spectra of the selected single minerals. This is natural, because a pixel in an LWIR image may be occupied by a single mineral instead of a mixture. Altogether, 55 LWIR spectra were used for the modelling. The additional single mineral spectra were actinolite, albite, biotite, calcite, chlorite, dolomite, diopside, epidote, hornblende, K-feldspar, muscovite, phlogopite, plagioclase, quartz, serpentine, talc and tremolite. The resulting accuracy of the pixel image interpretation is expected to be somewhat lower than the result in the previous section for the mean spectra, because the pixel spectra are noisier than the mean spectra. The results are illustrated in Figures 13 and 14 for those minerals that received reliable measures in the previous section.

A tentative test to predict chemistry and mineralogy from the Pyhäsalmi drilling powder samples

The hyperspectrally LWIR-imaged sample tray also contained a set of exploration drilling powders (37 samples) collected in 2001 (pers. comm. Timo Mäki 2001). All of them were chemically analysed for Cu, Zn and S, and 23 of them were also analysed for their mineralogy by MLA. The same methods were tentatively applied to these samples,

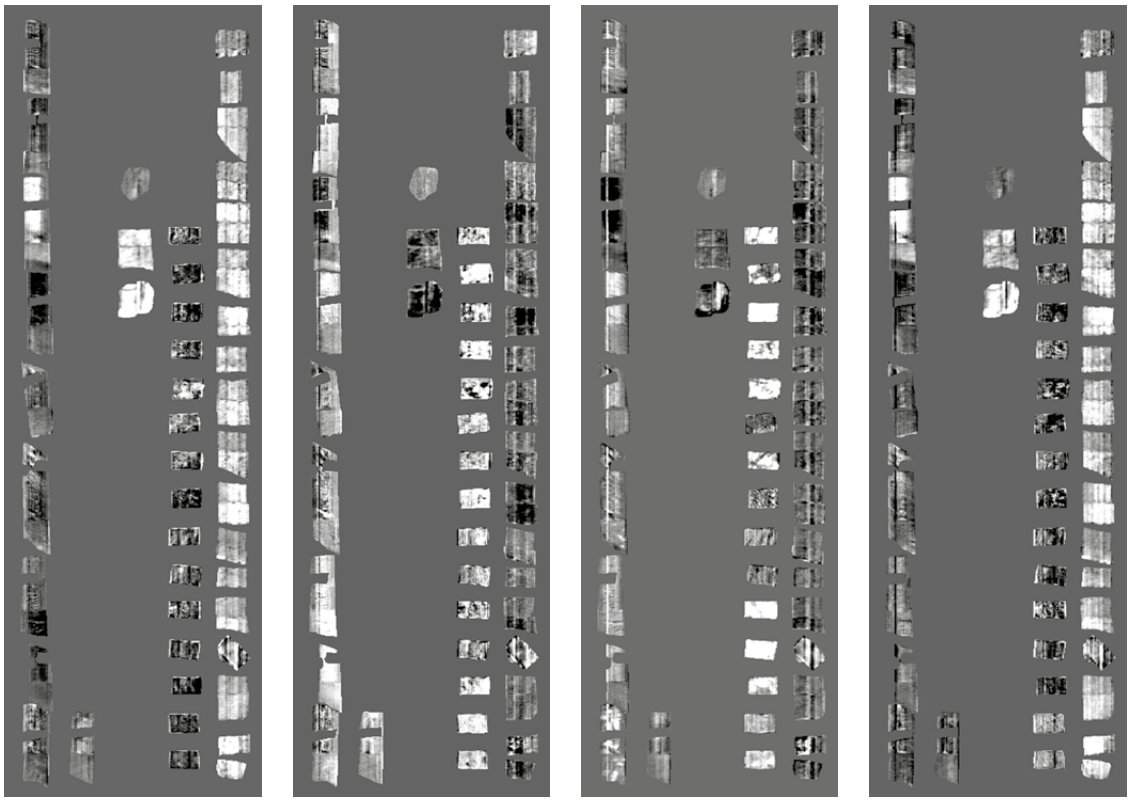

Albite Biotite Cordierite K-feldspar

Fig. 13. The first four main minerals predicted from the Pyhäsalmi-Kedonojankulma LWIR image by the PLSR model. The greytone variation limits from black to white for the minerals are: Albite 0.0-100.0%, Biotite 0.0-66.3%, Cordierite 0.0-78.6% and K_feldspar 0.0 -100.0%

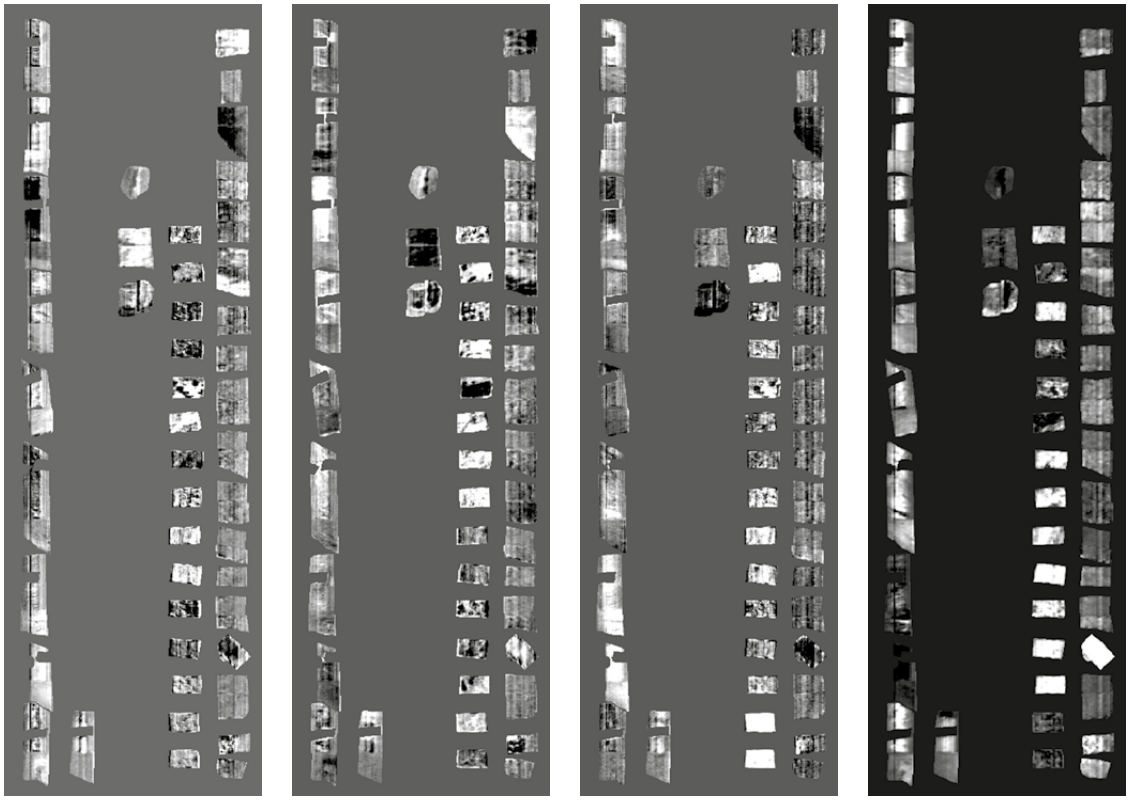

Muscovite Phlogopite Plagioclase Quartz

Fig. 14. The last four main minerals predicted from the Pyhäsalmi-Kedonojankulma LWIR image by the PLSR model. The greytone variation limits for the minerals are: Muscovite 0.0-100.0%, Phlogopite 0.0-53.6%, Plagioclase 0.0-87.7% and Quartz 0.0-100.0%

Pyhäsalmi_Powder_element prediction

Element index	Element	PLS MAE%	PLS RMSE%	PLS CC	Predictv ROIs	S-area [au]	p-value
1	**Zn**	**2.37**	**3.15**	**0.69**	**35**	**94.14**	**0.0000**
2	**S**	**11.50**	**14.94**	**0.49**	**35**	**1299.90**	**0.0023**
3	Cu	0.63	0.81	0.32	35	26.13	0.0610
Total area [au]						**1420.17**	

Table 5. Prediction parameters concerning the Pyhäsalmi drilling powder elements. The statistical error parameters suggest that the estimates are significant for Zn and S, but erroneous for Cu.

Pyhäsalmi_Powder_mineral prediction

Mineral index	Mineral	PLS MAE%	PLS RMSE%	PLS CC	Predictv ROIs	S-area [au]	p-value
1	**Actinolite**	**0.17**	**0.21**	**0.55**	**22**	**2.64**	**0.00604**
2	Albite	4.44	5.63	0.10	22	18.76	0.6587
3	Andalusite	0.31	0.60	-0.20	22	2.53	0.3663
4	Andradite	1.52	1.99	0.17	22	11.56	0.4275
5	Anthophyllite	0.26	0.43	-0.01	22	1.91	0.9702
6	**Apatite**	**0.09**	**0.12**	**0.52**	**22**	**1.27**	**0.0106**
7	Augite	0.43	0.57	0.27	22	3.70	0.2205
8	**Baryte**	**1.88**	**2.22**	**0.96**	**22**	**140.37**	**0.0000**
9	**Biotite**	**5.41**	**6.42**	**0.42**	**22**	**83.64**	**0.0455**
10	**Calcite**	**1.78**	**2.27**	**0.51**	**22**	**39.56**	**0.0138**
11	Celsian	0.73	1.12	-0.05	22	3.61	0.8208
12	Chalcopyrite	2.82	3.56	0.09	22	56.41	0.6984
13	Chlorite	5.55	7.05	-0.07	22	28.71	0.7342
14	**Clay_minerals**	**0.46**	**0.80**	**0.67**	**22**	**11.93**	**0.0004**
15	Clinozoisite	0.55	0.96	0.15	22	6.42	0.5016
16	**Cordierite**	**1.51**	**3.17**	**0.55**	**22**	**30.90**	**0.0069**
17	Diopside	1.63	2.27	0.29	22	19.32	0.1785
18	**Dolomite**	**1.60**	**3.15**	**0.68**	**22**	**30.57**	**0.0003**
19	Fe_oxide	2.15	2.69	-0.16	22	20.46	0.4670
20	**Gedrite**	**0.68**	**0.98**	**0.47**	**22**	**14.18**	**0.0246**
21	**Gypsum**	**0.60**	**0.78**	**0.55**	**22**	**10.70**	**0.0060**
22	Hornblende	2.21	3.38	0.29	22	27.85	0.1865
23	Hyalophane	0.51	1.15	-0.11	22	4.74	0.6264
24	**K_feldspar**	**0.25**	**0.35**	**0.84**	**22**	**4.91**	**0.0000**
25	Muscovite	5.85	13.79	-0.04	22	57.54	0.8601
26	Phlogopite	0.72	0.98	0.41	22	10.66	0.0533
27	**Plagioclase**	**6.63**	**9.09**	**0.76**	**22**	**149.01**	**0.0000**
28	**Pyrite**	**11.47**	**15.21**	**0.85**	**22**	**1070.53**	**0.0000**
29	Pyrrhotite	2.58	3.08	0.05	22	90.45	0.8274
30	**Quartz**	**2.32**	**2.98**	**0.93**	**22**	**127.67**	**0.0000**
31	**Serpentine**	**0.18**	**0.23**	**0.61**	**22**	**2.62**	**0.0019**
32	**Sphalerite**	**3.30**	**3.94**	**0.92**	**22**	**164.53**	**0.0000**
33	Talc	1.64	3.93	-0.09	22	18.92	0.6833
34	Tremolite	2.54	4.31	-0.03	22	26.50	0.8990
35	**Unclassified**	**0.06**	**0.08**	**0.57**	**22**	**2.49**	**0.0047**
	Total area [au]					**2297.55**	

Table 6. Prediction parameters concerning the Pyhäsalmi drilling powder minerals. The statistical error parameters suggest that the estimates for bolded minerals are acceptable.

however, bearing in mind that the samples were 'old', i.e., the surfaces of the sulphide minerals had oxidized into other chemical compounds during the 14 years of storage. The ore concentrates were not useful in this study, because the grains were covered by unknown non-mineral material. The results for the elements Cu, Zn and S are presented in Table 5. The results are, however, interesting: the elements S and Zn could be estimated with moderate accuracy (MAE ≤ 11.5%, CC ≥ 0.49, p-value ≤ 0.023), but Cu analysis was not successful. The reason is apparently that Cu has a very small variance in comparison with Zn and S, and that the surfaces of chalcopyrite may have suffered most due to oxidation.

The drilling powders were also subject to PLSR modelling with LWIR data for quantitative estimation of minerals. Those minerals that provided reliable quantity estimates are printed in bold in Table 6: actinolite, apatite, baryte, biotite, calcite, clay minerals, cordierite, dolomite, gedrite, gypsum, K-feldspar, plagioclase, pyrite, quartz, serpentine, sphalerite, and 'unclassified'. The presence of the class 'unclassified' means that there may exist a constant spectral signal from this material. Unfortunately, chalcopyrite and pyrrhotite dropped out due to high p-values or a low correlation between the predicted and measured quantities. The reason for this may be that the chalcopyrite and pyrrhotite area units [au] are small in the MLA data and that the mineral surfaces were oxidized. However, the reliably estimated minerals of the powders comprise 1888 au from the total 2298 au.

CONCLUSIONS

The SisuROCK LWIR imaging spectrometry reflectance data on rock samples was tested for ability to identify minerals and predict the mineral composition of samples. Three diverse targets were purposefully selected to test the method in versatile mineral/rock identification problems. The targets were the Kemi chromite mine, Pyhäsalmi Cu-Zn-S mine and Kedonojankulma Cu-Au ore prospect. In Kemi, the aim was to study the ore types and a few host rocks. In Pyhäsalmi and Kedonojankulma, the main focus of the study was on the identification of the alteration minerals among other minerals. A set of exploration drilling powders from Pyhäsalmi was also included in the study. They were analysed for minerals and the main chemical commodities.

The PLSR prediction result was successful for those minerals that were 'sufficiently present', i.e. comprising several percent; these could be quantitatively predicted. The reliability for their quantities and the error measures can be seen from the statistics performed. The following minerals were well quantified. They are, starting from the most reliably predicted (based on the low p-values with low or moderate MAEs), in the following list:

- Risk 0.0–1.1% (p-value x 100): albite, chromite, dolomite, magnesite, quartz, serpentine, talc, cordierite, muscovite, plagioclase, baryte, pyrite, sphalerite, K-feldspar, actinolite, tremolite, clay minerals, phlogopite, ilmenite, epidote, biotite, gypsum, apatite and laumontite.
- Risk 1.2–4.5% (p-value x 100): calcite, gedrite and chalcopyrite.
- Risk 5% (p-value x 100): chlorite

Chlorite covers a notable area in the MLA assays, but it could not be quantified with less than 5% risk. Besides chlorite, those minerals that classify the ore types and wall rocks (Kemi case) and the alteration minerals, among others (Pyhäsalmi and Kedonojankulma cases), are included in the list above.

The estimation of minerals for the drilling powders was less successful than for the solid rocks: all abundant minerals could be estimated with moderate accuracy, except pyrrhotite and chalcopyrite. The estimation of chemical elements for powders was analogous: Zn and S received moderate estimates, but not Cu. The reason for this may be that the powder samples were 14 years old and the surfaces of the mineral grains were therefore oxidized, masking the proper pyrrhotite and chalcopyrite.

As stated in the methodology section of this paper, literally negative prediction quantities occur. They illustrate the inadequacy of the sample set used for modelling in relation to the sample set to be interpreted, or the inadequacy of the spectral signature. In practical applications, the negative values are simply converted to zero, but a better option for further work is to prepare a perfect sample set and good reference data for exact regression modelling. The good reliability measures with

acceptable residuals between the predicted and measured quantities are frequently related to those minerals and/or samples that are well represented within the area exposed to the spectrometer.

The accuracy for the sample composition (ROI) prediction is seemingly better than the accuracy for single mineral prediction on average. The reason for this is that the quantities of the rare minerals are naturally small and they do not greatly affect the ROI spectra and the statistical measures. The UMXR and PLSR methods were compared for all predicted minerals in Kemi and Pyhäsalmi-Kedonojankulma cases. PLS and UMXR produced statistically very coincident results.

The main minerals, including the alteration minerals, and the unknown new mixtures of the minerals can be quantified using this LWIR & PLSR technique with accuracy, which would benefit mineral exploration and mining actions. LWIR imaging spectrometry is a rapid method for providing a quantitative estimation of the geological targets and sample compositions over large surfaces, presuming that the conditions for the prediction are carefully prepared. The key to success in quantifying a set of minerals is that the minerals have independent spectral LWIR signatures, the same minerals/rocks used in models become imaged by LWIR and MLA. It is also important that the model samples cover the variation of the mixtures of minerals.

ACKNOWLEDGEMENTS

Mr Ossi Leinonen (Avesta Polarit Oy), Mr Timo Mäki (Pyhäsalmi Mine Oy), Mr Timo Huhtelin (Outokumpu Ferrochrome Oy) and Mr Jukka Kousa (Geological Survey of Finland) are thanked for providing access to their mineral/rock sample materials. Dr Maarit Middleton (Geological Survey of Finland) and Dr Markus Törmä (Finnish Environment Institute) are gratefully acknowledged for reviewing this paper and helping to improve its structure and content. Mr Jukka Laukkanen, Ms Tuula Saastamoinen and Ms Neea Heino (all at the Geological Survey of Finland) are thanked for the MLA assays. Mr Harri Kutvonen (Geological Survey of Finland) is thanked for helping to prepare the graphics for this report.

REFERENCES

Abrams, M., Abbott, E. & Kahle, A. 1991. Combined use of visible, reflected infrared, and thermal infrared images for mapping Hawaiian lava flows. Journal of Geophysical Research—Solid Earth and Planets 96, 75–484.

Alapieti, T. T. 2005. Early Palaeoproterozoic (2.5-2.4 Ga) Tornio – Näränkävaara Layered Intrusion Belt and Related Chrome and Platinum-group Element Mineralization, Northern Finland. Chapter 1 in: Alapieti, T. T. & Kärki, A .J. (eds). Guide 51a, Geological Survey of Finland, 20 p. [Electronic resource]. Available at: http://tupa.gtk.fi/julkaisu/opas/op_051a_pages_013_032.pdf.

Alapieti, T. T. & Huhtelin, T. A. 2005. The Kemi intrusion and associated chromitite deposit. Chapter 2 in Alapieti, T. T. & Kärki, A. J. (eds). Guide 51a, Geological Survey of Finland, 20 p. [Electronic resource]. Available at: http://tupa.gtk.fi/julkaisu/opas/op_051a_pages_013_032.pdf.

Baldridge, A. M., Hook, S. J., Grove, C .I. & Rivera, G. 2009. The ASTER spectral library version 2.0. Remote Sensing of Environment 113, 711–715.

Bolin, B. J. & Moon, T. S. 2003. Sulfide detection in drill core from the Stillwater Complex using visible/near-infrared imaging spectroscopy. Geophysics 68, 1561–1568.

Brown, A. J., Sutter, B. & Dunagan, S. 2008. The MARTE VNIR Imaging Spectrometer experiment: design and analysis. Astrobiology 8, 1001–1011.

Gallie, E. A., Mcardle, S., Rivard, B. & Francis, H. 2002. Estimating sulphide ore grade in broken rock using visible/infrared hyperspectral reflectance spectra. International Journal of Remote Sensing 23, 2229–2246.

Geladi, P. &. Kowalski, B. R. 1986. "Partial least-squares regression: a tutorial," Analytica Chimica Acta, vol. 185, 1–17.

Hecker, C., Dilles, J. H., Mejde, M. van der & Meer, F. D. van der. 2012. Thermal infrared spectroscopy and partial least squares regression to determine mineral modes of granitoid rocks, Geochemistry Geophysics Geosystems, vol. 13 (3), 1–15.

Hook, S. J. & Kahle, A. B. 1996. The micro Fourier Transform Interferometer (mu FTIR)—a new field spectrometer for acquisition of infrared data of natural surfaces. Remote Sensing of Environment 56, 172–181.

Iljina, M. & Hanski, E. 2005. Layered mafic intrusions of the Torni-Näränkävaara belt. In: Lehtinen, M. Nurmi, P. A. & Rämö, O .T. (eds). 2005. Precambrian Geology of Finland – Key to the Evolution of the Fennoscandian Shield. Elsevier B.V., Amsterdam, 101–138.

Kirkland, L., Herr, K., Keim, E., Adams, P., Salisbury, J., Hackwell, J. & Treiman, A. 2002. First use of an airborne

thermal infrared hyperspectral scanner for compositional mapping. Remote Sensing of Environment 80, 447–459.

Korsman, K., Koistinen, T., Kohonen, J., Wennerström, M., Ekdahl, E., Honkamo, M. , Idman, H. & Pekkala, Y. (eds). 1997. Suomen kallioperäkartta – Berggrundskarta över Finland – Bedrock map of Finland 1 : 1 000 000, Geological Survey of Finland, Espoo, Finland.

Kousa, J., Luukas, J., Mäki, T., Ekdahl, E., Pelkonen, K., Papunen, H., Isomäki, O.-P., Penttilä, V.-J. & Nurmi, P. 1997. Geology and mineral deposits of the central Ostrobothnia. Geological Survey of Finland, Guide 41, 43–67.

Kouvo, O. 1977. The use of mafic pegmatoids in geochronometry. Abs. 5th. Europ. Coll. Geochrom, Pisa, Italy.

Krämer, N. & Sugiyama, M. 2011. The Degrees of Freedom of Partial Least Squares Regression. Journal of the American Statistical Association. vol.106, no.494, pp.697{705, 2011. [Electronic resource]. Available at: http://citeseerx.ist.psu.edu/viewdoc/download?doi=10.1.1.386.4679&rep=rep1&type=pdf . Last accessed 23 June 2015.

Kruse, F. A. 1996. Identification and mapping of minerals in drill core using hyper spectral image analysis of infrared reflectance spectra. International Journal of Remote Sensing 17, 1623–1632.

López-Alonso, J. M. & Alda, J. 2002. Bad pixel identification by means of principal component analysis. Optical Engineering 41, 2152–2157.

Mäki, T. 1986. Lithogeochemistry of the Pyhäsalmi zinc-copper-pyrite deposit, Finland. In: Prospecting in Areas of Glaciated Terrain 1986. Kuopio, Finland, 1–2 September 1986. London: The Institution of Mining and Metallurgy, 69–82.

Mason, P. & Huntington, J. F. 2012. HyLogger 3 components and pre-processing: An overview. Northern Territory Geological Survey, Technical Note 2012-002. 9 p.

Mevik, B.-H. & Wehrens, R. 2007. The pls Package: Principal component and Partial Least Squares Regression in R. Journal of Statistical Software. Vol 18, Issue 2, 1–24.

Middleton, M., Närhi, P., Kuosmanen, V., & Sutinen, R. 2011. Quantification of glacial till chemical composition by reflectance spectroscopy. Applied Geochemistry 26 (2011) 2215-2225.

Nielsen, A. A. 1999. Linear Mixture Models, Full and Partial Unmixing in Multi- and Hyperspectral Image Data.

Pratt, W. K. 2001. Digital Image Processing. Wiley & Sons, 738 p.

Puustjärvi, H. (ed.) 1999. Pyhäsalmi Modelling Project. Technical Report 13.5.1997 – 12.5.1999. 251 p., 76 app. [Electronic resource]. Available at: http://tupa.gtk.fi/raportti/arkisto/m19_3321_99_1_10.pdf.

Råde, L. & Westergren, B. 2004. Mathematics Handbook for Science and Engineering. Studentlitteratur, Lund, Sweden. 562 p.

Ragona, D., Minster, B., Rockwell, T. & Jussila, J. 2006. Field imaging spectroscopy: a new methodology to assist the description, interpretation, and archiving of paleoseismological information from faulted exposures. Journal of Geophysical Research-Solid Earth 111.

Salisbury, J. W. & Daria, D. M. 1992. Emissivity of terrestrial materials in the 8-14 MUM atmospheric window. Remote Sensing of Environment 42, 83–106.

Salisbury, J. W., Walter, L. S. & Vergo, N. 1989. Availability of a library of infrared (2.1–25.0 MU-M) mineral spectra. American Mineralogist 74, 938–939.

Sylvester, P. J. 2012. Chapter 1: use of the mineral liberation analyzer (MLA) for mineralogical studies of sediments and sedimentary rocks. Mineralogical Association of Canada Short Course 42, St. John's NL, May 2012, 1–16

Taranik, J., Riley, D., Hackwell, J., Vaughan, G. & Aslett, Z. 2008. Development of hyperspectral thermal remote sensing for geological applications. International Geological Congress, Oslo. [Electronic resource]. Available at: http://www.cprm.gov.br/33IGC/1342506.html. Last accessed 23 June 2015.

Tiainen, M., Kärkkäinen, N., Lohva, J., Sipilä, P. & Huhta, P. 2012. Discovery of the Kedonojankulma Cu-Au occurrence, hosted by a Svecofennian porphyritic granitoid in Southern Finland. Geological Survey of Finland, Special Paper 52, 73–90.

Tiainen, M., Molnar, F. & Koistinen, E. 2013. The Cu-Mo-Au mineralization of the Paleoproterozoic Kedonojankulma intrusion, Häme Belt, Southern Finland. 12th Biennial SGA Meeting, Uppsala, Sweden.

van der Meer, F. 2006. The effectiveness of spectral similarity measures for the analysis of hyperspectral imagery. International Journal of Applied Earth Observation and Geoinformation 8, 3–17.

Wold, H. 1975. Path models with latent variables: the NIPALS approach. In: Blalock, H. M. et al. (eds). Quantitative sociology: international perspectives on mathematical and statistical modeling, Academic, 307–357.

Wold, S., Sjöström, M. & Eriksson, L. 2001. PLS-regression: a basic tool of chemometrics, Chemometrics and Intelligent Laboratory Systems 58 (2), 109–130.